Combination of long-term 13CO2 labeling and isotopolog profiling allows turnover analysis of photosynthetic pigments in Arabidopsis leaves

Anh Thi-Mai Banh
IBG-2: Plant Sciences, Forschungszentrum Jülich
Björn Thiele
IBG-2: Plant Sciences, Forschungszentrum Jülich
Antonia Chlubek
IBG-2: Plant Sciences, Forschungszentrum Jülich
Thomas Hombach
IBG-2: Plant Sciences, Forschungszentrum Jülich
Einhard Kleist
IBG-2: Plant Sciences, Forschungszentrum Jülich
Shizue Matsubara (s.matsubara@fz-juelich.de)
IBG-2: Plant Sciences, Forschungszentrum Jülich

Method Article

Keywords: Carotene, Carotenoids, Chlorophyll, Lutein, Pigment metabolism, Stable isotope labeling, Turnover, 13CO2

Posted Date: May 18th, 2022

DOI: https://doi.org/10.21203/rs.3.rs-1405084/v1

<METHODOLOGY>

Combination of long-term $^{13}CO_2$ labeling and isotopolog profiling allows turnover analysis of photosynthetic pigments in Arabidopsis leaves

Anh Thi-Mai Banh[1], Björn Thiele[1,2], Antonia Chlubek[1], Thomas Hombach[1], Einhard Kleist[1], Shizue Matsubara[1]*

*Correspondence: s.matsubara@fz-juelich.de
[1]IBG-2: Plant Sciences, Forschungszentrum Jülich, 52425 Jülich, Germany
[2]IBG-3: Agrosphere, Forschungszentrum Jülich, 52425 Jülich, Germany

Abstract

Background: Living cells maintain and adjust structural and functional integrity by continual synthesis and degradation of metabolites and macromolecules. The maintenance and adjustment of thylakoid membrane involve turnover of photosynthetic pigments along with subunits of protein complexes. Quantifying their turnover is essential to understand the mechanisms of homeostasis and long-term acclimation of photosynthetic apparatus. Here we report methods combining whole-plant long-term $^{13}CO_2$ labeling and LC-MS analysis to determine the size of non-labeled population (NLP) of carotenoids and chlorophylls (Chl) in leaf pigment extracts of partially ^{13}C-labeled plants.

Results: The labeling chamber enabled parallel $^{13}CO_2$ labeling of up to 15 plants of *Arabidopsis thaliana* with real-time environmental monitoring ([CO_2], light intensity, temperature, relative air humidity and pressure) and recording during the experiment. No significant difference in growth or photosynthetic pigment composition was found in leaves after 7-d exposure to normal CO_2 (~400 ppm) or $^{13}CO_2$ in the labeling chamber, or in ambient air outside the labeling chamber (control). Following chromatographic separation of the pigments and mass peak assignment by high-resolution Fourier-transform ion cyclotron resonance mass spectrometry (MS), mass spectra of photosynthetic pigments were analyzed by triple quadrupole MS to calculate NLP. The size of NLP remaining after the 7-d $^{13}CO_2$ labeling was ~10.3% and ~11.5% for all-*trans*- and 9-*cis*-β-carotene, ~21.9% for lutein, ~18.8% for Chl *a* and 33.6% for Chl *b*, highlighting non-uniform turnover of these pigments in thylakoids. Comparable results were obtained in all replicate plants of the $^{13}CO_2$ labeling experiment except for three that were showing anthocyanin accumulation and growth impairment due to insufficient water supply (leading to stomatal closure and less ^{13}C incorporation).

Conclusions: Our methods allow $^{13}CO_2$ labeling and estimation of NLP for photosynthetic pigments with high reproducibility. The results indicate distinct turnover rates of carotenoids and Chls in thylakoid membrane, which can be investigated in the future by time course experiments. Since ^{13}C enrichment can be measured in a range of compounds, long-term $^{13}CO_2$ labeling chamber, in combination with appropriate MS methods, facilitates turnover analysis of various metabolites and macromolecules in plants on a time scale of hours to days.

Keywords: Carotene, Carotenoids, Chlorophyll, Lutein, Pigment metabolism, Stable isotope labeling, Turnover, $^{13}CO_2$

Background

Living cells need maintenance to preserve structural and functional integrity. The maintenance involves breakdown, (re)synthesis and active transport of molecules such as proteins and membrane lipids. While turnover (continual replacement by degradation and synthesis) of macromolecules – proteins in particular – is costly for cells, it allows adjustments of biochemical machinery to environmental changes [1].

Plants have relatively low rates of protein turnover compared to bacteria. Early investigations on protein turnover using $^{14}CO_2$ labeling have indicated turnover rate of approx. 0.1~0.2 d^{-1} in leaves of tobacco, bean, wheat and barley, whereas bacterial cells may have overall protein turnover of 1.2–1.4 d^{-1} [1]. More recently, proteomic studies using ^{15}N labeling have determined degradation rate (K_D; equivalent to turnover rate in a steady state) of numerous proteins, showing the median of 0.08 d^{-1} and 0.11 d^{-1} in barley and Arabidopsis leaves, respectively [2, 3]. The proteome analysis also highlighted great variations in K_D among proteins. In Arabidopsis leaves, in which K_D was estimated for 1228 non-redundant proteins, ~15% of the proteins had >0.22 d^{-1} whilst ~13% had <0.055 d^{-1} [3]. Among high-turnover proteins detected in both barley and Arabidopsis are THI1 (1.65 d^{-1} and 1.93 d^{-1} in barley and Arabidopsis, respectively) and THIC (0.64 d^{-1} and 0.89 d^{-1}) in thiamine biosynthesis, and D1 protein (0.94 d^{-1} and 1.08 d^{-1}) in photosystem II (PSII) reaction center [2, 3]. THI1 and D1 are considered "suicide proteins" because THI1 is a single-use enzyme that serves as a co-substrate by donating a sulfur atom of a cysteine [4, 5] and D1 acts as a safety device that is sacrificed to protect the rest of PSII against photooxidative damage [6–8].

Given the costs of protein turnover, one may ask: Are high-turnover proteins worth the benefits? Some attempts have been made to estimate the costs and benefits of D1 damage and repair in oxygenic photosynthesis [9, 10]. The calculation depends on the definition of costs (energy requirement for degradation and synthesis of protein and RNA, additional needs for N and P, missed opportunity for photosynthesis) and the extent of photodamage. The latter, in turn, is influenced by environmental conditions and efficacy of photoprotective mechanisms, including thermal energy dissipation, scavenging of reactive oxygen species, alternative electron transport pathways, state transitions and chloroplast movement [6, 9]. Should it be necessary to replace pigments and lipids in the reaction center and core complex of PSII during the D1 turnover, this would increase the costs of repair and maintenance [9]. A PSII core complex harbors in total 35 chlorophyll *a* (Chl *a*) molecules, two pheophytins, 11 all-*trans*-β-carotenes (β-Car), two plastoquinones, two haem irons and more than 20 lipids besides Mn, Ca, Cl and bicarbonate [11]. We must also keep in mind that not only D1 but also other proteins associated with photosynthesis, such as PetD of cytochrome b_6f complex and PIFI of chloroplast NAD(P)H dehydrogenase complex, have relatively high K_D values (>0.5 d^{-1}) in Arabidopsis [8].

Previously we have shown the turnover of Chl *a* and all-*trans*-β-Car in leaves of Arabidopsis plants under illumination [12, 13]. A 30-min pulse labeling with $^{14}CO_2$ resulted in rapid incorporation of ^{14}C in these pigments, whereas Chl *b* and xanthophylls were not labeled throughout the subsequent 10-h chase [12]. Treatment with lincomycin, an inhibitor of plastid translation and thus D1 synthesis, quickly and strongly suppressed ^{14}C incorporation in Chl *a*, and to a lesser extent also β-Car, suggesting a link to the D1 turnover [13]. Although detection of radioactive ^{14}C is highly sensitive as well as selective, turnover rates could not be determined in these studies due to the unknown number of $^{12}C/^{14}C$ substitution per molecule. For example, if all C atoms of Chl *a* and β-Car are labeled with ^{14}C, a molecule of Chl *a* ($C_{55}H_{72}O_5N_4Mg$) will have stronger radioactivity than a β-Car ($C_{40}H_{56}$). However, if Chl *a* is partially labeled, let us say 20 C atoms out of 55, its radioactivity is only a half of fully labeled β-Car. Another downside of our $^{14}CO_2$ labeling was the use of excised leaves to minimize radioactive wastes, which restricted the duration of the pulse-chase labeling experiments [12, 13].

^{13}C offers a good alternative to ^{14}C in these respects. ^{13}C is a stable, non-hazardous isotope that can be detected and quantified by mass spectrometry (MS). For each compound, mass spectra can show the relative abundance of individual isotopologs having different isotopic compositions (e.g. $^{13}C_{55}$, $^{12}C_{35}{}^{13}C_{20}$, $^{12}C_{55}$ etc. for Chls), thus enabling the counting of non-labeled and ^{13}C-labeled (fully or partially) molecules. As the first step to study turnover of photosynthetic pigments, we established a liquid chromatography (LC)-MS analysis method

for isotopolog profiling of carotenoids. This method, recently described in [14] for lutein (Lut), allows identification and quantification of isotopologs in ^{13}C-labeled leaf pigment extracts. Similar methods are also needed for Chls and other carotenoids to analyze turnover of these pigments in a single run. Furthermore, long-term whole-plant $^{13}CO_2$ labeling is ideally performed in a chamber, in which the environmental conditions can be controlled and monitored during labeling experiments. Such a chamber will open up new possibilities for turnover studies of many different compounds in plants.

Here we report a protocol of 7-d $^{13}CO_2$ labeling in a chamber that was specially designed and constructed for this type of experiments. We also describe the LC-MS analysis methods to identify isotopologs and calculate non-labeled population (NLP) of β-Car, Chl *a* and Chl *b* besides Lut in pigment extracts of ^{13}C-labeled leaves. With these methods of $^{13}CO_2$ labeling and isotopolog analysis at hand, turnover of photosynthetic pigments and other metabolites can be studied in the future by time course experiments.

Methods

Plant material and growth conditions

Plants of *Arabidopsis thaliana* (Columbia-0) were grown in 300-mL plastic cups with lids (Additional file 1; Fig. A1; Bürkle, Bad Bellingen, Germany) which tightly fit into holders of the labeling chamber described below. After cups had been filled with moist soil (Dachstaudensubstrat SoMi 513, Hawita, Vechita, Germany), 1–2 cm^3 of seed starting soil (Pikier Erde, Blaster Einheitserdewerk, Fröndenberg, Germany) was put in the center of the top soil where individual seeds were sown. Cotyledons grew out of the cup through a hole (3 mm diameter) made in the center of the lid. The lid thus separated the aboveground from root system and soil to minimize the impact of root and soil respiration on the CO_2 composition inside the labeling chamber. The lid (except the hole) was covered with aluminum foil to suppress algal growth on the soil surface. Two holes (~4.5 mm diameter; Additional file 1; Fig. A1) made in the bottom of the cups allowed bottom watering.

Plants were cultivated in a climate chamber under 12 h/12 h light/dark, 23°C/18°C air temperature and constant 60% relative air humidity. Illumination was provided by fluorescent tubes (Fluora L36 W/77, Osram, Munich, Germany) which gave light intensity of ~100 µmol photons m^{-2} s^{-1} at plant height. Care was taken to keep soil moisture by regular watering from the bottom. Five weeks after sowing, 15 plants of similar projected leaf area (PLA, 14–16 cm^2) were selected for a preliminary CO_2 experiment to develop a gas flow rate protocol (see below). Plants were transferred to the labeling chamber installed in a separate climate chamber. After

136 the flow rate protocol had been established, a new batch of plants were cultivated in the same
137 way and 19 plants having 14–16 cm^2 PLA were selected for a $^{13}CO_2$ experiment (day 0 in
138 Additional file 1; Figs. A2, A3a). Of these, 15 were placed in the labeling chamber while the
139 remaining four plants stayed outside the labeling chamber (control).
140 The rosettes of the 19 plants were individually harvested after seven light/dark cycles in
141 $^{13}CO_2$ or ambient air (day 8 in Additional file 1; Figs. A2, A3b). The rosettes were quickly
142 photographed for visual documentation before freezing in liquid N_2 for pigment analysis.
143
144 ## Measurement of PLA
145 During plant cultivation, PLA was determined daily by using the Growscreen-FLUORO
146 method [15] or by taking a top-view image of the plants. In the latter case, a blue reference chip
147 (2 cm diameter) was placed next to the plant (Additional file 1; Figs. A2–A4) to facilitate pixel-
148 to-area conversion. Images were analyzed by ImageJ [16] to obtain PLA.
149
150 ## $^{13}CO_2$ labeling
151 We constructed a chamber for long-term $^{13}CO_2$ labeling of small plants such as Arabidopsis
152 (Fig. 1). It is equipped with the following control and measuring devices: four mass flow
153 controllers (MFC1–MFC4; EL-FLOW F-201CV-10K-RAR-00-V, F-200C-RFB-33-Z, F-
154 201C-RFB-33-V, F-201CV-100-RAR-00-Z, Bronkhorst Deutschland Nord, Kamen, Germany)
155 for CO_2-free air and CO_2, an infrared gas analyzer (IRGA; LI-840, LI-COR, Lincoln, NE, USA)
156 to measure [CO_2], a custom-made dew point trap cooled by a water bath (6°C; Julabo F32 MA,
157 JULABO Labortechnik, Seelbach, Germany) to reduce air humidity, four fans (8412 NGMV,
158 EBM papst, Mulfingen, Germany) in four corners to mix the air inside the chamber, five
159 temperature sensors (type K, mawi-therm Temperatur-Prozeßtechnik, Essen, Germany) placed
160 in four corners and at the center, and one sensor each for air humidity (DKRF400,
161 Driesen+Kern, Bad Bramstedt, Germany), light intensity (LI-190R, LI-COR) and pressure
162 (M260 Multisense, Setra Systems, Boxborough, MA, USA).
163 The labeling chamber has 15 airtight holders for plant cups described above (Fig. 2a). The
164 chamber can be closed with a glass cover (50 x 88 x 16 cm; L x W x H) (Fig. 2b). The connection
165 between the glass cover and the chamber body is sealed with polyurethane foam gaskets
166 (Armaflex AF/E 10 mm, Armacell, Münster, Germany). As this sealing is not airtight, a small
167 overpressure is needed inside the labeling chamber to prevent diffusion of ambient air from the
168 outside (see below). The overpressure results in air leakage and thus a loss of $^{13}CO_2$ from the
169 chamber through the glass cover sealing. A shallow plastic basin attached to the lower surface

of the chamber body can be filled with water through a tubing (Fig. 2b) without opening the chamber. When plant cups are put in the holders, the bottom of the cups touches the water in the basin, thus allowing bottom watering.

While the labeling chamber is in operation, two gas pumps (NMP830KVDCB and N 816 K_DC-B, KNF Neuberger, Freiburg, Germany) continuously circulate the internal air through bypasses that lead to LI-840 and the dew point trap (Fig. 1). The flow rates of the gas pumps were set to 1 L min^{-1} (to LI-840) and 14 L min^{-1} (to the dew point trap). The four MFCs are controlled by a custom-made computer program (made with LabVIEW 2014; National Instruments, Austin, TX, USA), which also visualizes environmental readings of the sensors in real time and records the data every minute. The flow rates of MFC2 (CO_2 or $^{13}CO_2$) and MFC3 (CO_2-free air prepared by filtering the ambient air through an industrial adsorption dryer KEN-MT 3800 MSTE; Parker Hannifin, Kaarst, Germany) were adjusted such that [CO_2] of ~400 ppm was maintained during the light period (Additional file 1; Fig. A5a–c). The mass flow of CO_2-free air (1 L min^{-1} or 2 L min^{-1}) created a small overpressure (~60 Pa or 160-170 Pa; Additional file 1; Fig. A5d) inside the labeling chamber compared to the outside (atmospheric pressure, ~101.3 kPa) to prevent diffusion of external air into the chamber. The amount of CO_2 injection was increased as the light intensity increased in the morning (see below for light intensity regime) and as the plants grew larger (Additional file 1; Fig. A5b). To keep daytime [CO_2] constant, the amount of CO_2 injection must be balanced with net CO_2 fixation of the plants, which depends on the genotype, size (leaf area) and development, as well as the conditions during cultivation and labeling.

We did not inject CO_2 during the dark period (except during 20-min equilibration immediately before the onset of light period; see below) while the flow of CO_2-free air was increased from 1 L min^{-1} to 2 L min^{-1} (Additional file 1; Fig. A5a, b) to minimize accumulation of respired CO_2 with unknown degree of ^{13}C labeling. As a result, nocturnal [CO_2] decreased to below 100 ppm (Additional file 1; Fig. A5c). Since plants were grown in the ambient air, we set the flow rate of CO_2-free air to 2 L min^{-1} during the first light period when light respiration of $^{12}CO_2$ was expected to dilute $^{13}CO_2$. The flow rate of CO_2-free air was reduced to 1 L min^{-1} during the subsequent light periods (presumably decreasing $^{12}CO_2$ in respiration) to lower the overpressure and thus reduce the loss of $^{13}CO_2$ from the labeling chamber. During the dark periods, the high flow rate of CO_2-free air and thus the high overpressure (Additional file 1; Fig. A5d) effectively blocked the diffusion of external air into the chamber. Should the overpressure exceed a given threshold (250 Pa in this study), a safety valve would open automatically to release the air from the chamber. This threshold, however, was never reached

during the experiments (Additional file 1; Fig. A5d). In addition to the high flow rate during the dark periods, the labeling chamber was flushed with CO_2-free air (MFC1; 10 L min^{-1} for 45 min) at the end of each dark period to get rid of nocturnal air containing respiratory CO_2 of unknown isotopic composition. The flushing was followed by 20-min equilibration with a fresh mixture of CO_2 (MFC4; 5 mL min^{-1}) and CO_2-free air (MFC1; 10 L min^{-1}) immediately before the onset of the light period. An outlet valve was automatically opened during flushing and equilibration to keep the overpressure low.

We conducted a preliminary experiment using normal CO_2 (purchased from Air Products, Hattingen, Germany) to establish a flow rate protocol (Additional file 1; Figs. A2, A6). This protocol was then used in the experiment with $^{13}CO_2$ (>99 atom %; Linde, Pullach, Germany). Since LI-840 has a very low sensitivity to $^{13}CO_2$ [17], the readings were low in the $^{13}CO_2$ experiment (Additional file 1; Fig. A6). Nevertheless, light/dark patterns of [CO_2] were highly reproducible in both CO_2 and $^{13}CO_2$ conditions, suggesting that the flow rate protocol provided similar [CO_2] inside the labeling chamber.

The labeling chamber was placed under LED lamps (L4A Series 10, HelioSpectra, Göteborg, Germany) in the climate chamber running with 12 h/12 h light/dark and constant 20°C and 60% relative air humidity. The intensity of LED lamps was increased or decreased in three steps at the beginning or at the end of the 12-h light period, respectively (Additional file 1; Fig. A7a). The light period started with 30-min dim light (~28 µmol photons m^{-2} s^{-1}), followed by an increase to ~115 µmol photons m^{-2} s^{-1} (60 min) and then to ~200 µmol photons m^{-2} s^{-1} (9 h) before returning to darkness in the reverse sequence. The light intensity shown in Additional file 1; Fig. A7a was measured by LI-190R mounted near the plant position P7 and P8 (see Figs. 1, 2) in the closed chamber (i.e., under the glass cover). Figure 2a illustrates light distribution in the open chamber measured at plant height using X1 optometer (Gigahertz-Optik, Türkenfeld, Germany). The mean intensity of the 15 plant positions was 238 µmol photons m^{-2} s^{-1} ±10% SD without the glass cover. Comparing the values measured at around P7 and P8 in the open and closed chamber, the glass cover apparently reduced the light intensity by ca. 25%. For the control plants outside the labeling chamber, the intensity of LED was set to the level similar to the condition in Additional file 1; Fig. A7a.

While the climate chamber had constant 20°C and 60% relative air humidity, illumination and plant transpiration raised the air temperature and humidity inside the closed labeling chamber (Additional file 1; Fig. A7b, c). The air temperature increased to ~23°C during the light period and decreased to ~20.5°C during the dark period. Although the chamber has a dew point trap (Fig. 1), the capacity of the dew point trap was not enough to fully compensate for

238 the transpiration of 15 growing plants of Arabidopsis; the air humidity gradually increased from
239 ~55% to ~75% during the 7-d experiments even though the chamber was flushed daily and the
240 flow rate of CO_2-free air was kept at 2 L min^{-1} during the dark periods.
241 The $^{13}CO_2$ labeling was stopped after seven light/dark cycles. The chamber was opened in
242 the dim light at the beginning of the light period of day 8 to harvest the whole rosette of each
243 plant. As opening the chamber inevitably exposes plants to ambient air, we collected all plants
244 (also the control) during the 30-min dim-light period to minimize photosynthetic CO_2 fixation.
245 The total amount of $^{13}CO_2$ used by the flow rate protocol (including daily flushing, equilibration
246 and loss in addition to CO_2 assimilation of 15 plants) during the 7-d labeling was ca. 6.8 L.
247
248 ## Pigment extraction
249 The whole rosettes of Arabidopsis plants were individually frozen in liquid N_2 and ground to
250 powder using pre-cooled mortar and pestle. They were stored at -80°C until pigment extraction.
251 About 40 or 80 mg of frozen leaf powder were quickly weighed with an analytical balance
252 (Explorer Pro, OHAUS, Nänikon, Switzerland). Pigments were extracted by using the protocol
253 described before [14]. The weighed frozen leaf powder was ground in 2 mL of chilled acetone
254 under dim light and the homogenate was collected in a 2-mL reaction tube. After 5-min
255 centrifugation at 16,100 rcf (5415D, Eppendorf, Wesseling-Berzdorf, Germany), the
256 supernatant was filtered through a syringe filter (0.45 µm, Chromafil® AO-45/3, Macherey-
257 Nagel, Düren, Germany) into a brown glass vial. All extracts were prepared shortly before
258 injection into LC-MS instruments.
259
260 ## MS analysis
261 The LC-MS system consists of a Waters ACQUITY UPLC system and a Waters Xevo TQ-S
262 triple quadrupole MS (hereafter TQ-MS). The LC-Fourier-transform ion cyclotron resonance-
263 MS (hereafter FTICR-MS) consists of an Agilent 1200 series HPLC system and a hybrid linear
264 ion trap FTICR-MS (LTQ FT Ultra, Thermo Fisher Scientific) equipped with a 7 Tesla magnet.
265 Soft ionization was performed in positive ion mode by electrospray ionization (ESI in TQ-MS)
266 or atmospheric pressure chemical ionization (APCI in FTICR-MS). For information about the
267 instrument settings, see [14].
268 Chromatographic separation was done by a C30 silica column (ProntoSil 200-3-C30, 250 x
269 4.6 mm, 3 µm, Bischoff Chromatography, Leonberg, Germany) using the method described in
270 [14]. Pigments were identified based on absorption spectra. Chromatograms were extracted at
271 440 nm and peak area integration was performed by MassLynx software (version 4.1, Waters)

for TQ-MS data. To determine pigment concentration, the LC of the TQ-MS system was calibrated with pigment standards purchased from DHI LAB products (Hørsholm, Denmark): Lut, all-*trans*-α-Car, all-*trans*-β-Car, Chl *a* and Chl *b* as well as 9-*cis*-neoxanthin (Neo), violaxanthin (Vio), antheraxanthin (Anthera) and zeaxanthin (Zea). Carotenoid levels relative to Chl (Chl *a* + Chl *b*) were calculated in mmol mol^{-1} Chl. The de-epoxidation state (DES) of the xanthophyll-cycle pigments was defined as (Anthera + Zea) / (Vio + Anthera + Zea).

Mass spectra were obtained at the maximal intensity of the pigment peaks in ion chromatograms (FTICR-MS) or by manually selecting the regions around the maximal peak intensity (TQ-MS) using a full scan mode to cover mass-to-charge ratio (*m*/*z*) between 350 and 1000. Data were processed with MassLynx for TQ-MS and Xcalibur (version 2.0.7, Thermo Fisher Scientific) for FTICR-MS. We first analyzed one each of the ^{13}C-labeled and non-labeled (control) samples using both TQ-MS and FTICR-MS to assign mass peaks. The high mass accuracy of FTICR-MS allows assignment of mass peaks to distinct empirical formulae. The resolving power (full width at half maximum) of FTICR-MS was 100,000 at *m*/*z* 400. Based on the peak assignment of FTICR-MS, matching peaks were identified in the corresponding data of TQ-MS. All other samples were analyzed by TQ-MS using the same peak selection schemes.

Degree of ^{13}C labeling (DoL) and NLP of pigments

The base peak intensity (BPI) was calculated for each pigment isotopolog as follows [14]:

$$BPI_i = \frac{I_i}{I_{(max)}} \cdot 100 \qquad \text{Eqn. 1}$$

where BPI_i is the base peak intensity of an isotopolog with i ^{13}C atoms, i the number of ^{13}C atoms in the isotopolog, I_i the peak intensity of an isotopolog with i ^{13}C atoms, and $I_{(max)}$ the highest peak intensity of all isotopologs of the pigment.

The BPI_i values were then normalized to the sum of BPI_i of all isotopologs of the pigment.

$$BPI_{i(norm)} = \frac{BPI_i}{\sum_{i=0}^{n} BPI_i} \cdot 100 \qquad \text{Eqn. 2}$$

$BPI_{i(norm)}$ is the normalized base peak intensity of an isotopolog with i ^{13}C atoms and n is the number of C atoms in the pigment molecule (40 for carotenoids, 55 for Chls).

The DoL was calculated for each isotopolog as follows:

$$DoL_i = \frac{BPI_{i(norm)} \cdot i}{n} \qquad \text{Eqn. 3}$$

where DoL_i is the degree of ^{13}C labeling of an isotopolog with i ^{13}C atoms.

The overall DoL (ΣDoL) of the pigment can be obtained by adding up DoL_i of all isotopologs.

$$\Sigma DoL = \sum_{i=0}^{n} DoL_i \qquad \text{Eqn. 4}$$

We estimated the relative abundance of non-labeled pigment population (NLP), which can be defined as the sum of $BPI_{i(norm)}$ of all non-labeled isotopologs. Due to natural abundance of ^{13}C in the atmosphere (1.1%), isotopologs having a few ^{13}C atoms are always found in plant extracts (Additional file 1; Fig. A8). These naturally ^{13}C-containing isotopologs were considered "non-labeled".

Spike test of TQ-MS

Pigment recovery of the TQ-MS system was checked by spike tests. About 40 mg of frozen leaf powder of a ^{13}C-labeled Arabidopsis plant were homogenized in 2 mL of chilled acetone. The homogenate was then divided into two aliquots and 0.5 mL of pigment standards (Lut, all-*trans*-β-Car and Chl *a*; all from DHI LAB products) of known concentrations were spiked in one aliquot. Both aliquots were centrifuged and the supernatants filtered into brown glass vials as described above. Following TQ-MS analysis of the pigment standards and the ^{13}C-labeled Arabidopsis leaf pigment extract with and without spike (Additional file 1; Fig. A9), $BPI_{i(norm)}$ was calculated for the pigments using Eqn. 2. Because addition of non-labeled standards should increase the relative abundance of non-labeled isotopologs in the spiked sample, recovery of the added standards can be estimated from the ratio between the measured and the expected increase in NLP of the spiked sample compared to the non-spiked sample.

$$Recovery = \frac{measured\ NLP\ increase}{expected\ NLP\ increase} \qquad \text{Eqn. 5}$$

The results of the spike tests are documented in Additional file 2; Table 1. The recovery was 95% or higher for all three pigments.

Reproducibility of ΣDoL and NLP

Technical reproducibility of ΣDoL and NLP was verified by repeated injections of a ^{13}C-labeled Arabidopsis pigment extract into TQ-MS and analyzing ΣDoL and NLP in these data. The mean values (±SD with n=3 for all-*trans*-βCar, Lut and Chl *a*, n=4 for Chl *b*) of ΣDoL and NLP thus obtained for each pigment are summarized in Additional file 2; Table 2.

Results

$^{13}CO_2$ treatment in the labeling chamber

The labeling chamber was first run with normal CO_2 to establish a flow rate protocol of CO_2 and CO_2-free air (see the description in Methods). This was necessary because LI-840, which was connected to the labeling chamber (Fig. 1), measures [CO_2] at the wavelength of ~4.26 µm

where $^{12}CO_2$ absorbs much more strongly than $^{13}CO_2$ (Additional file 1; Fig. A6) [17]. Subsequently, the $^{13}CO_2$ labeling experiment was conducted using the same protocol.

Figure A2 in Additional file 1 shows top-view images of the plants at the beginning (day 0) and at the end of the experiment (day 8). Grown in the same conditions, the plants with similar PLA looked very much alike on day 0. After seven light/dark cycles in the normal CO_2 or $^{13}CO_2$ conditions inside the labeling chamber, the plants were visually indistinguishable from the control plants that stayed in the ambient air outside the labeling chamber. The chamber has 15 plant cup holders for simultaneous labeling (Fig. 2). All 15 plants of the $^{13}CO_2$ experiment are shown in Additional file 1; Fig. A3. Three plants (P6, P13 and P15) grew less and showed anthocyanin accumulation during the experiment (Fig. 2b); their plastic cups were not placed deep enough in the holders, resulting in suboptimal watering and stomatal closure, and thus less CO_2 fixation and growth. No sign of stress was recognized in other 12 plants. For comparison, the pictures of 15 plants used in the preliminary experiment with normal CO_2 are shown in Additional file 1; Fig. A4. Two plants (P9 and P11) were somewhat smaller at the end of the preliminary experiment. Overall, however, growth and visual phenotype of the plants were comparable between the $^{13}CO_2$ and normal CO_2 experiments.

Leaf pigment composition was analyzed in the 15 plants of the $^{13}CO_2$ experiment as well as four control plants. The ^{13}C-labeled plants and non-labeled control were comparable regarding leaf carotenoid and Chl contents (Fig. 3), except that two control plants had somewhat higher DES of the xanthophyll-cycle pigments (Fig. 3d). Since the leaves were harvested under dim light in the morning, all samples had high levels of Vio, some Anthera and only trace amounts of Zea (Fig. 3b, c). The pigment composition did not systematically differ between the stressed plants (P6, P13 and P15) and the rest.

Mass peak assignment and calculation of DoL and NLP

The substitution of ^{12}C (mass 12.000000) by ^{13}C (mass 13.003355) and *vice versa* can be detected in molecules by MS analysis. In order to identify pigment isotopologs in mass spectra of ^{13}C-labeled samples, mass peaks were assigned to empirical formulae by high-resolution FTICR-MS. Matching peaks were then selected in the corresponding data of TQ-MS. Since mass peak assignment of Lut is explained elsewhere [14], we describe below the procedures of peak assignment and analysis focusing on β-Car and Chls. We could not analyze mass spectra of Zea due to the low concentrations in the samples (Fig. 3b); peak assignment of Vio, Anthera and Zea will be reported in a separate study. The MS analysis of Neo was confronted by co-eluting compounds.

Chromatographic separation of photosynthetic pigments was monitored at 440 nm (Fig. 4a). The ion chromatograms presented in Fig. 4b–g were extracted at nominal mass of monoisotopic pigment ions: $^{12}C_{40}$ for carotenoids and $^{12}C_{55}$ for Chls. Since ionization occurred in positive mode, $[M+H]^+$ was the major quasi-molecular ion of Vio (Fig. 4b) and Chls (Fig. 4d, f). Lut has strong tendency to lose water upon protonation [14, 18, 19], forming $[M+H–H_2O]^+$ as the main quasi-molecular ion (Fig. 4e). Vio also gave rise to multiple dehydration products ($–H_2O$, $–2H_2O$ or $–3H_2O$) but $[M+H]^+$ was still the most abundant ion. In contrast to xanthophylls, both all-*trans* and 9-*cis* isomers of β-Car predominantly formed $[M]^+$ in TQ-MS (Fig. 4g) and $[M+H]^+$ in FTICR-MS (see below).

Figure 5 collates mass spectra of all-*trans*-β-Car in the non-labeled and ^{13}C-labeled samples analyzed by FTICR-MS and TQ-MS. Similar mass spectra, albeit with stronger backgrounds, were also obtained for the less abundant 9-*cis*-β-Car (Additional file 1; Fig. A10). The mass peaks of β-Car are clustered around *m/z* 536–537 in the non-labeled sample (Fig. 5a, b; Additional file 1; Fig. A10a, b). After the 7-d $^{13}CO_2$ treatment, a second peak cluster comprising ^{13}C-labeled isotopologs emerged at around *m/z* 575–576 (Fig. 5c, d; Additional file 1; Fig. A10c, d). The peaks of ^{13}C-labeled isotopologs were much higher than the non-labeled ones, indicating that the majority of β-Car, both all-*trans* and 9-*cis*, were newly synthesized during the $^{13}CO_2$ treatment.

We selected the mass peaks of all-*trans*-β-Car isotopologs in the TQ-MS data (Additional file 2; Tables A4, A6) as per the peak assignment of FTICR-MS in the non-labeled and ^{13}C-labeled samples (Additional file 2; Tables A3, A5). Due to limited mass resolution, TQ-MS cannot distinguish mass peaks of $[M]^+$ and $[M+H]^+$ ions when they have similar *m/z* values following $^{12}C/^{13}C$ substitution (Δ mass = 1.003355) or protonation (Δ mass = 1.007276). FTICR-MS, at the resolving power used (100,000 at *m/z* 400), could separate most of the β-Car peaks in the ^{13}C-labeled cluster, while it failed to resolve a few peaks in the non-labeled cluster (Additional file 2; Tables A3–A6). In case of overlap, peaks were regarded as the more abundant form. Thus, overlapping peaks of $[M]^+$ and $[M+H]^+$ were considered $[M]^+$ in the TQ-MS analysis and $[M+H]^+$ in the FTICR-MS analysis of β-Car. This led to a small overestimation of β-Car ΣDoL by TQ-MS because $[M]^+$ has one more ^{13}C atom compared to $[M+H]^+$ at similar *m/z* (e.g. $[^{12}C_{39}{}^{13}C\text{-}M]^+$ and $[^{12}C_{40}\text{-}M+H]^+$). Consequently, ΣDoL values of all-*trans*-β-Car were slightly higher when calculated from the TQ-MS data (ca. 1.4% and 86.1% for non-labeled and ^{13}C-labeled sample, respectively) instead of the FTICR-MS data (ca. 1.2% and 84.2%) (Additional file 2; Tables A3–A6). Using the same peak assignment, we found comparable ΣDoL for 9-*cis*-β-Car shown in Additional file 1; Fig. A10: ca. 1.2% and 84.7% for non-labeled

405 and ^{13}C-labeled sample by TQ-MS, ca. 1.0% and 82.1% by FTICR-MS. Note that the peaks of
406 all-*trans*- and 9-*cis*-β-Car were not completely separated in the ion chromatogram (Fig. 4g),
407 which may partly explain the similar ΣDoL of these isomers.
408 Next, we estimated the size of NLP based on the relative abundance of non-labeled β-Car
409 isotopologs in the ^{13}C-labeled sample (i.e., the sum of $BPI_{i(norm)}$ in the white cells of Additional
410 file 2; Tables A5, A6). For calculation of NLP, it should not matter whether unresolved peaks
411 of β-Car are considered $[M]^+$ or $[M+H]^+$ because the overlaps occurred exclusively within the
412 non-labeled or the ^{13}C-labeled peak cluster. Nevertheless, TQ-MS gave a somewhat smaller
413 NLP of all-*trans*-β-Car (ca. 10.3%) than FTICR-MS did (ca. 12.2%) (Additional file 2; Tables
414 A5, A6). The same also applied to 9-*cis*-β-Car (ca. 11.5% and 14.3% by TQ-MS and FTICR-
415 MS, respectively). NLP is always 100% in non-labeled control.
416 We followed the same procedure to assign the mass peaks of Lut. As already mentioned,
417 $[M+H–H_2O]^+$ is the predominant ion of Lut (Fig. 6) [14, 18, 19]. FTICR-MS separated all mass
418 peaks of Lut detected in non-labeled and ^{13}C-labeled samples (Additional file 2; Tables A7,
419 A9), while TQ-MS showed overlaps between $[M]^+$ and $[M+H]^+$ in both non-labeled and ^{13}C-
420 labeled *m/z* regions (Additional file 2; Tables A8, A10). Since the overlapping peaks in the TQ-
421 MS data were considered $[M+H]^+$, ΣDoL of Lut was slightly underestimated by TQ-MS in both
422 non-labeled and ^{13}C-labeled samples (ca. 1.0% and 74.1%, respectively) compared to FTICR-
423 MS (ca. 1.3% and 75.0%) (Additional file 2; Tables A7–A10). Conversely, NLP was marginally
424 overestimated by TQ-MS in the labeled sample (ca. 21.9% vs 21.0% by FTICR-MS).
425 Unlike carotenoids, which are made solely of C and H (carotenes) or C, H and O
426 (xanthophylls), Chls also contain N and Mg. While natural abundance of ^{2}H (0.02%), ^{17}O
427 (0.04%), ^{18}O (0.2%) and ^{15}N (0.4%) are all low, two stable isotopes of Mg (^{25}Mg 10%, ^{26}Mg
428 11%) exist in significant amounts in nature alongside the most abundant ^{24}Mg (79%). Peak
429 assignment and analysis of Chl mass spectra must take into account Mg isotopes (^{24}Mg/^{25}Mg Δ
430 mass = 1.000795; ^{24}Mg/^{26}Mg Δ mass = 1.997551) in addition to ^{12}C/^{13}C substitution and
431 protonation. Furthermore, the number of possible formulae increases with increasing molecular
432 mass. As a result, Chl mass spectra were difficult to analyze even by FTICR-MS. Moreover,
433 formation of $[M+K]^+$ adduct was seen in both FTICR-MS and TQ-MS data of Chl *a* (Fig. 7),
434 and TQ-MS data of Chl *b* (Fig. 8b, d). Some TQ-MS data also showed a trace of $[M+Na]^+$ in
435 ^{13}C-labeled samples. To simplify the analysis of Chl mass spectra, we focused on the $[M+H]^+$
436 ion of ^{24}Mg-Chl because ^{13}C labeling of Chl should be independent of the type of ion produced
437 by MS instruments and of the Mg isotope inserted in the protoporphyrin IX during Chl
438 biosynthesis. The relative contributions of ^{24}Mg-Chl, ^{25}Mg-Chl and ^{26}Mg-Chl to overlapping

mass peaks were calculated based on the natural abundance of these Mg isotopes. As the peaks of non-labeled $[M+K]^+$ and ^{13}C-labeled $[M+H]^+$ were partly overlapping (Figs. 7c, d and 8d), we estimated the intensity of non-labeled $[M+K]^+$ peaks from the intensity of non-labeled $[M+H]^+$ peaks in the same data, assuming the relative abundance of $[M+K]^+$ and $[M+H]^+$ peaks found in the non-labeled control (Figs. 7a, b and 8b). The intensity of non-labeled $[M+K]^+$ was then subtracted from the overlapping peaks to obtain the intensity of ^{13}C-labeled $[M+H]^+$.

The peak assignment and calculation of Chl *a* and Chl *b* are summarized in Additional file 2; Tables A11–A18. For comparison, calculation is reported for both $[M+H]^+$ and $[M+K]^+$ ions in the non-labeled control (Additional file 2; Tables A11, A12, A16). As expected, ΣDoL did not substantially differ between the two ionization products ($[M+H]^+$ and $[M+K]^+$). Between the two instruments, TQ-MS gave higher ΣDoL for both non-labeled and ^{13}C-labeled samples compared to FTICR-MS; the values obtained in the labeled sample were ca. 67.3% and 70.4% for Chl *a* (by FTICR-MS and TQ-MS; Additional file 2; Tables A13, A14) and ca. 54.9% and 57.5% for Chl *b* (Additional file 2; Tables A17, A18). The TQ-MS data underestimated NLP of Chl *a* in the ^{13}C-labeled sample (ca. 18.8% and 20.7% by TQ-MS and FTICR-MS), whereas their NLP values were similar for Chl *b* (ca. 33.6% and 33.0%).

Overall, ΣDoL and NLP were largely comparable between the TQ-MS and FTICR-MS data, with deviations ranging between less than one and a few points after the 7-d $^{13}CO_2$ labeling. Also the technical reproducibility was high for both parameters (Additional file 2; Table A2).

Variations in ΣDoL and NLP among the 15 plants in the $^{13}CO_2$-labeling experiment

We analyzed ΣDoL and NLP in all samples using TQ-MS. Figure 9a shows box plots of ΣDoL. Three plants had lower ^{13}C enrichment in the pigments; these were P6, P13 and P15 that displayed anthocyanin accumulation and reduced growth (Additional file 1; Fig. A3b). The smallest plant (P13) had the lowest ΣDoL for all pigments. Apart from these three, the other ^{13}C-labeled plants were similar in terms of ΣDoL (Fig. 9a). β-Car had the highest average ΣDoL (86.5% ±2.2 SD for all-*trans*; 85.4% ±1.6 for 9-*cis*) and Chl *b* the lowest (59.4% ±4.5). The ΣDoL was comparable for Lut (72.9% ±2.8) and Chl *a* (71.5% ±4.0). Notably, P13 showed substantially lower ΣDoL for Chl *a* (ca. 18.9%) than for Lut (ca. 36.4%).

NLP (Fig. 9b) shows a mirror image of ΣDoL (Fig. 9a). As seen for ΣDoL, the NLP values were similar in all ^{13}C-labeled plants but the three (P6, P13 and P15). After the 7-d labeling, the average NLP of the 12 plants was no more than 9.9% ±2.2 for all-*trans*-β-Car and 10.8% ±1.6 for 9-*cis*-β-Car (Fig. 9b). These values are about a half of Chl *a* (18.9% ±3.2) and Lut

(23.5% ±2.9) or 1/3 of Chl *b* (33.0% ±4.3). The smallest plant (P13) had the largest NLP for all pigments, showing again a large difference between Chl *a* (ca. 70.7%) and Lut (ca. 60.3%).

Having seen the non-uniform ^{13}C enrichment patterns in different pigments of the ^{13}C-labeled plants (Fig. 9), we made pairwise comparisons of NLP between the pigments (Fig. 10). All four comparisons revealed a positive linear correlation but the slope of regression lines differed. The slope was roughly one in the comparison between the two Chls, although NLP was always smaller for Chl *a* than for Chl *b* (Fig. 10a). The correlation between the two carotenoids had a slope of less than 0.9 (Fig. 10b), suggesting a smaller variation in Lut per unit change in all-*trans*-β-Car. The Chl-carotenoid comparisons, i.e., Chl *a vs* all-*trans*-β-Car (Fig. 10c; slope ~0.8) and Chl *b vs* Lut (Fig. 10d; slope <0.7), indicated larger variations for Chls than for carotenoids among the 15 plants. Yet, NLP was consistently smaller for carotenoids than for Chls. The same comparisons made for ΣDoL (Additional file 1; Fig. A11) displayed the same trends in the opposite direction.

The large variations in NLP and ΣDoL found between the non-labeled and ^{13}C-labeled plants as well as between the non-stressed and stressed plants (Figs. 9, 10; Additional file 1; Fig. A11) are in marked contrast to the similarity in their pigment composition (Fig. 3).

Discussion

Chamber for long-term $^{13}CO_2$ labeling

$^{13}CO_2$ labeling offers a means to trace the fate of carbon assimilated by photoautotrophic organisms. After fixation into sugars, further metabolization can be detected by GC-MS, LC-MS or NMR [20–22] to study the networks of carbon metabolism in plant tissues. The interest in metabolic flux analysis has been growing in plant research, despite the challenges that are inherent to multi-compartment cells and multicellular samples [23–26]. For instance, $^{13}CO_2$ pulse-chase experiments have been conducted for flux analysis of central metabolism in intact leaves and whole Arabidopsis rosettes [27–31]. For short-term (seconds to minutes) labeling to capture rapid ^{13}C incorporation and enrichment in primary metabolites, labeling chambers and leaf cuvettes must have a small volume to ensure minimal time lag after switching between ambient CO_2 and $^{13}CO_2$ [27–31]. Some chambers also allow instant quenching (flash-freezing) to preserve metabolic state of the sample. Small labeling chambers and cuvettes were also used to track ^{13}C down the plastidic 2*C*-methyl-D-erythritol-4-phosphate (MEP) pathway and isoprene biosynthesis [32–36].

$^{13}CO_2$ labeling is an established approach in plant research to investigate phenomena that develop over hours and days or even weeks and months. Ecological and ecophysiological

studies, such as investigation of above- and belowground carbon allocation in trees [37–40], employ $\delta^{13}C$ measurements by isotope ratio mass spectrometer following *in situ* $^{13}CO_2$ labeling. The $\delta^{13}C$ method can also be employed for laboratory experiments to trace metabolization and translocation of ^{13}C-labeled assimilates [41]. When combined with hydroponic cultivation, dual labeling with $^{13}CO_2$ and ^{15}N (in the form of $^{15}NH_4NO_3$, $^{15}NH_4{}^{15}NO_3$ or $K^{15}NO_3$ in nutrient solution) enables simultaneous tracking of C and N allocation [41]. While ^{15}N feeding was successfully applied to unveil leaf proteome turnover [2, 3], attempts are being made with $^{13}CO_2$ to concomitantly analyze turnover of metabolites and proteins [42, 43]. Chambers for long-term $^{13}CO_2$ labeling typically have a large volume to treat multiple plants in parallel [41–44]. Even an entire walk-in climate chamber can be used for $^{13}CO_2$ labeling [45], budget permitting. In order to both monitor and control the conditions during the experiments, long-term labeling chambers are often equipped with environmental sensors and control devices [41, 42, 44].

The choice of chamber design depends on research goals and available resources. Our labeling chamber for long-term turnover analysis belongs to the latter type. It has a volume of ca. 70 L for simultaneous labeling of up to 15 small plants and is furnished with temperature, humidity, light and pressure sensors besides the IRGA for measuring [CO_2] (Figs. 1, 2). Due to the low sensitivity of LI-840 for $^{13}CO_2$, a preliminary experiment with normal CO_2 was necessary to establish a labeling protocol (Additional file 1; Figs. A5, A6). Installation of an IRGA or other instrument that can measure $^{13}CO_2$ would allow direct control of [$^{13}CO_2$] and thus do away with the prior CO_2 experiment. If a $^{13}CO_2$ gas analyzer is not available, as was the case in the present work, flow rate protocols developed in normal CO_2 can be used to reproduce the experimental conditions in $^{13}CO_2$. It is then imperative that very similar plants be used in both CO_2 and $^{13}CO_2$ experiments (Additional file 1; Fig. A2-A4). Also, the importance of homogenous conditions inside the chamber (Fig. 2a) cannot be stressed enough; environmental heterogeneity can have cumulative effects on $^{13}CO_2$ labeling of plants (replicates) over a long period. In the labeling experiment, except for the visibly stressed P6, P13 and P15, the other plants were similar in terms of visual phenotype (Additional file 1; Fig. A3), pigment composition (Fig. 3) as well as NLP and ΣDoL (Fig. 9). Although [$^{13}CO_2$] was not measured in this study, our chamber and experimental protocols apparently provided adequate conditions for long-term $^{13}CO_2$ labeling.

NLP of carotenoids

Similar ΣDoL and NLP values of the non-stressed plants (Fig. 9) underscore high reproducibility (both technical and biological) of the methods. Whilst the number of unresolved

mass peaks was greater in the TQ-MS data than in the FTICR-MS data (Additional file 2; Tables A3–A18), high pigment recovery and reproducibility of the TQ-MS system could be validated (Additional file 2; Tables A1, A2). Below, we discuss NLP of carotenoids (Lut and β-Car) and Chls (Chl *a* and Chl *b*) obtained by TQ-MS.

Previously we described a method of Lut isotopolog profiling in ^{13}C-labeled leaf pigment extracts [14]. Using the method, NLP was calculated for Lut extracted from leaves of the 7-d ^{13}C-labeled Arabidopsis plants (Fig. 9b). The data of the non-stressed plants are scattered around the median, which was much lower than the NLP in the stressed plants. The deviations between the TQ-MS-based and FTICR-MS-based NLP are <1 point for Lut, despite the unresolved peaks in the TQ-MS data at *m/z* 569–571 and *m/z* 607–608 (Additional file 2; Tables A8, A10) [14]. This is because none of the overlapping peaks belongs to the predominant ion $[M+H–H_2O]^+$. The relative intensity ($BPI_{i(norm)}$) of the overlapping peaks is too low to affect ΣDoL and NLP substantially. Moreover, the overlaps between $[M]^+$ and $[M+H]^+$ are of no consequence to NLP when they appear within non-labeled or labeled peak cluster; only the peak assignment of small overlaps between non-labeled and labeled isotopologs at *m/z* 569–571 affects the calculation of NLP. The relative intensity in this *m/z* region is no more than 3% of the total, about a half of which is assigned to non-labeled $[M]^+$ and $[M+H]^+$ and the other half to ^{13}C-labeled $[M+H–2H_2O]^+$ (Additional file 2; Table A9). When the abundance of the latter diminishes in less strongly labeled samples (e.g. in experiments with shorter labeling), between-cluster peak overlap will not be an issue for Lut.

Given that all ionization products must have the same ^{13}C labeling pattern, an alternative way to analyze Lut data is to avoid overlapping peak regions altogether and use only $[M+H–H_2O]^+$, which constitutes >80% of our Lut mass spectra (Fig. 6; Additional file 1; Fig. A9a–c). The NLP values thus calculated are ca. 20.9% and 20.6%, respectively, for the FTICR-MS and TQ-MS data shown in Additional file 2; Tables A9, A10, instead of ca. 21.0% and 21.9% considering all four ions. Regardless of whether the calculation includes all ions or only $[M+H–H_2O]^+$, similar NLP values can be obtained for Lut, with very minor differences between FTICR-MS and TQ-MS. We note that peak assignment and calculation of DoL and NLP basically follow the same procedures for all xanthophylls that are typically found in chloroplasts.

New in the present study is the assignment of β-Car and Chl isotopolog peaks to enable turnover analysis of different pigments in the same sample. Two well-separated peak clusters characterize the mass spectra of all-*trans*-β-Car in ^{13}C-labeled samples (Fig. 5c, d; Additional file 1; Fig. A9d–f): a labeled cluster at around *m/z* 575-576 and a non-labeled cluster at around *m/z* 536-537. The latter reflects the natural abundance of ^{12}C/^{13}C, as seen in the control (Fig.

5a, b) and predicted by the simulation (Additional file 1; Fig. A8). Since the unresolved mass peaks of β-Car appear solely within non-labeled or labeled cluster, they should not affect the calculation of NLP. Even so, TQ-MS slightly underestimated NLP of β-Car in the ^{13}C-labeled sample (ca. –1.9 and –2.8 points for all-*trans*- and 9-*cis*-β-Car, respectively) compared to FTICR-MS. The discrepancy between the two instruments declines to ca. 1.1 and 1.7 points when NLP of the FTICR-MS data is calculated from the major $[M+H]^+$ ion alone, rather than both $[M]^+$ and $[M+H]^+$ (Additional file 2; Table A5).

All-*trans*-β-Car is the predominant form of Car in PSII and PSI [11, 46]. While α-Car may also be found in leaf pigment extracts, especially (but not only) in shade-tolerant species [47, 48], the α-Car level is typically low in Arabidopsis leaves. Strong light and heat can trigger *cis-trans* isomerization in carotenoids [49, 50], which can be separated by C_{30} reversed-phase HPLC column [51, 52]. In the present study, we had moderate light and temperature conditions in the labeling chamber (Additional file 1; Fig. A7a, b) and pigments were extracted in chilled acetone under dim light. Still, 9-*cis*-β-Car and 9-*cis*-Neo were detected in all samples (Fig. 4a). Formation of these 9-*cis* isomers was specific, as neither 13-*cis* and 15-*cis* isomers of β-Car and Neo nor any *cis* isomers of Vio, Anthera and Lut were found. In fact, 9-*cis*-β-Car is a native constituent of cytochrome b_6f complex [53–55]. Binding of 9-*cis*-Neo to PSII light-harvesting antenna complexes is also well-established [56–59]. Interestingly, even though the two β-Car isomers differ greatly in the concentration (Fig. 4a), their NLP values after the 7-d $^{13}CO_2$ labeling were equally low (Fig. 9b).

NLP of Chls

The ^{13}C-labeled isotopolog peaks are more broadly distributed than non-labeled ones. This broadening is particularly manifest in the mass spectra of Chls (Figs. 7c, d and 8c, d) consisting of a porphyrin ring and a phytol side chain. At the center of porphyrin is Mg with three naturally abundant isotopes (^{24}Mg, ^{25}Mg and ^{26}Mg), which, however, hardly broadens the mass spectra of non-labeled Chls (Figs. 7a, b and 8a, b). The broadening of Chl mass spectra is therefore solely ascribable to ^{13}C enrichment. In accordance, similarly broad mass spectra were reported for ^{13}C-labeled pheophytin following the removal of Mg from ^{13}C-labeled Chl [60].

The peak cluster of ^{13}C-labeled Chls extends over a wide *m/z* region, with the strongly labeled isotopologs ($^{13}C_{55}$ to $^{12}C_{15}{}^{13}C_{40}$) accounting for a large part of ΣDoL (Additional file 2; Tables A13, A14, A17 and A18). The labeled $[M+H]^+$ cluster is tailing off at lower *m/z*, as can be recognized in Figs. 7 and 8 despite the partial overlap with non-labeled $[M+K]^+$ peaks. The mass peaks in this low *m/z* region have been attributed to isotopologs having ^{13}C-labeld

porphyrin with non-labeled phytol or ^{13}C-labeled phytol with non-labeled porphyrin [60]. Our Chl mass spectra revealed a small sub-cluster at around $^{12}C_{35}{}^{13}C_{20}$ (*m/z* ~913 for Chl *a* and ~927 for Chl *b;* Figs. 7 and 8), corresponding to non-labeled porphyrin with ^{13}C-labeled phytol. The existence of this sub-cluster is most evident in the absence of $[M+K]^+$ in the FTICR-MS data of Chl *b* (Fig. 8c). In contrast, mass peak distribution was continuous for ^{13}C-labeled porphyrin with non-labeled phytol, suggesting variable ^{13}C enrichment patterns of the porphyrin moiety synthesized from glutamate.

Glutamate is rather slowly labeled by $^{13}CO_2$ and also slowly unlabeled during subsequent chase in ambient CO_2 [28, 41, 42]. In comparison, glyceraldehyde-3-phosphate and pyruvate, the two precursors of plastidic isoprenoid biosynthesis via the MEP pathway leading to carotenoids and phytol, are rapidly labeled by $^{13}CO_2$ in illuminated leaves [28]. The Chl molecules comprising labeled and non-labeled moieties are thought to arise from recycling of de-esterified chlorophyllide and phytol [60]. By using radioactive ^3H-labeling, incorporation of phytol in Chl and tocopherol has been demonstrated in Arabidopsis seedlings [61]. It should be noted, however, that Chl molecules, which are "newly" synthesized from recycled chlorophyllide and recycled phytol, will be indistinguishable from preexisting "old" molecules based on their mass. Should such complete recycling occur, it would result in overestimation of NLP. How often Chl molecules are recycled in leaves is unknown. According to our data from the 7-d labeled Arabidopsis leaves, the relative abundance of isotopologs with labeled and non-labeled moieties was 5–9% of the total Chl pool (Figs. 7 and 8; Additional file 2; Tables A13, A14, A17 and A18). Similar values (<10%) were also found for pheophytin prepared from Chl *a* of *Synechocystis* sp. PCC 6803 after 2-d labeling with ^{13}C-glucose and $H^{13}CO_3^-$ [60].

We were unable to resolve all peaks in the pigment mass spectra, in particular for Chls (Additional file 2; Tables A11–A18). Higher resolving power than was used in this study would be desirable for better peak assignment. The analysis of Chl mass spectra can be simplified through Mg removal by weak acid treatment [60], although this will require separate sample preparation and analysis for Chls and carotenoids. Formation of alkali metal adducts is a common phenomenon for some compounds in positive ion mode. We estimated the contribution of $[M+K]^+$ in the overlapping peak region of ^{13}C-labeled Chl mass spectra (Figs. 7c, d and Fig. 8d) based on the $[M+K]^+$:$[M+H]^+$ ratio found in the control (Figs. 7a, b and Fig. 8b). This ratio was highly reproducible in the mass spectra of the four control plants (±6–8% SD for Chl *a*, ±4% SD for Chl *b*). We assumed that the ^{13}C-labeled plants had similar levels of K (hence also similar $[M+K]^+$:$[M+H]^+$ ratios) in leaves. As K contents may vary in different tissues, genotypes and species under different conditions, careful choice of control is essential

642 to estimate the relative intensity of $[M+K]^+$ peaks in this way. Additionally, the choice of
643 ionization technique can partly ameliorate the problem with alkali metal adducts [62]; in the
644 present study, APCI (in FTICR-MS) induced less alkali metal adduction than ESI did (in TQ-
645 MS) (Figs. 7 and 8).
646 The calculation based on $[M+H]^+$ of ^{24}Mg-Chl indicated ca. 18.8% and 20.7% NLP for Chl
647 *a* (by TQ-MS and FTICR-MS, respectively) and ca. 33.6% and 33.0% for Chl *b* (Additional
648 file 2; Tables A13, A14, A17 and A18). The discrepancy between the two instruments is
649 somewhat larger for Chl *a* (ca. 2.2 points) and β-Car (ca. 1.1 and 1.7 points for all-*trans* and 9-
650 *cis*) than for Chl *b* and Lut (<1 point). In view of the variations among the non-stressed replicate
651 plants shown in Fig. 9b, this level of under- or overestimation is within a tolerable range.
652
653 ## Different NLP of carotenoids and Chls
654 Cells synthesize new molecules as they grow. Growth-driven incorporation of ^{13}C strongly
655 dilutes NLP in long-term labeling experiments. After the 7-d $^{13}CO_2$ labeling, all pigments had
656 larger NLP in the stressed plants (Fig. 9b) showing reduced growth (Additional file 1; Fig. A3b).
657 If growth is the only process that dilutes NLP and there is no change in pigment concentration,
658 the entire set of pigments is expected to show more or less the same decline in NLP. Yet, our
659 analysis revealed distinct NLP for carotenoids and Chls (Fig. 9b), suggesting different turnover
660 of these pigments.
661 Our previous studies using radioactive $^{14}CO_2$ labeling have shown the turnover of Chl *a* and
662 all-*trans*-β-Car in mature leaves of Arabidopsis in the light [12, 13]. Both pigments had ^{14}C
663 incorporation already after 30-min pulse labeling, whereas Chl *b* and xanthophylls did not. The
664 rapid labeling of Chl *a* and all-*trans*-β-Car without changes in their concentration is indicative
665 of high turnover, presumably in connection with the D1 damage and repair [12, 13]. The D1
666 protein of PSII reaction center is known to undergo high turnover in illuminated leaves [6–8].
667 Some of the Chl *a* and all-*trans*-β-Car molecules, which are bound in the reaction center and
668 core complex of PSII [11], seem to be degraded and replaced by newly synthesized molecules
669 during the repair cycle. Between the two, all-*trans*-β-Car had a smaller NLP after the 7-d $^{13}CO_2$
670 labeling (Figs. 9b, 10c). This may be explained by different localization of these pigments;
671 while all-*trans*-β-Car is mostly bound to the core complexes of PSII and PSI [11, 46], Chl *a* is
672 universally found in all photosynthetic pigment-protein complexes. The proportion of
673 molecules undergoing turnover in PSII is thus larger for all-*trans*-β-Car than for Chl *a*.
674 Moreover, NLP of Chl *a* may be underestimated due to complete recycling of chlorophyllide
675 and phytol, should this happen. Analogously, lower NLP of Lut compared to Chl *b* (Figs. 9b,

10d), the two pigments that co-localize in light-harvesting antenna complexes [56–59, 63], may be a sign of Chl recycling, although higher turnover of Lut cannot be ruled out. If 9-*cis*-β-Car is specifically bound to cytochrome b_6f complex [53–55], the similar NLP values found for all-*trans*- and 9-*cis*-β-Car (Fig. 9b) may imply medium turnover of 9-*cis*-β-Car in cytochrome b_6f, i.e., not as high as all-*trans*-β-Car in PSII but higher than that in PSI. Yet, given the incomplete chromatographic separation of all-*trans*- and 9-*cis*-β-Car (Fig. 4g), their mass spectra (Fig. 5; Additional file 1; Fig. A10) may contain some signals from each other. Better separation is needed to estimate NLP of the less abundant 9-*cis*-β-Car (Fig. 4a).

Conclusions

With these combined methods for long-term $^{13}CO_2$ labeling and parallel determination of pigment concentration and NLP established, it is now possible to study photosynthetic pigment turnover. While we did not do time course analysis, the results presented in Figs. 9 and 10 point to distinct turnover rates of carotenoids and Chls. Future experiments, including the xanthophyll-cycle pigments that were left out of the scope of this study, could throw light on active maintenance and adjustment of photosynthetic pigments in leaves. Since changes in ^{13}C enrichment can be analyzed in a wide range of compounds using appropriate MS methods, long-term $^{13}CO_2$ labeling chamber, like the one described above, can facilitate investigations of dynamic turnover of various metabolites and macromolecules in plants on a time scale of hours to days.

Acknowledgements

We thank Andreas Fischbach (IBG-2, Forschungszentrum Jülich) for his support with Growscreen-FLUORO, Olaf Gardeick (IBG-2) for supply of CO_2-free air, and Diana Hofmann (IBG-3) for discussion on mass spectra.

Authors' contributions

SM designed the experiments. EK designed the labeling chamber. EK, AC and TH installed the sensors and other devices of the labeling chamber. AC made the computer program. AT-MB and SM tested the labeling chamber. AT-MB, BT and SM performed experiments and analyzed data. SM and AT-MB wrote the manuscript. All authors read and approved the final manuscript.

Funding

A. T.-M. Banh is a recipient of the MOET scholarship (Ministry of Education and Training, Vietnam). This work was supported by the Deutsche Forschungsgemeinschaft (DFG, project ID 391465903/GRK 2466).

Availability of data and materials

The datasets obtained and/or analyzed during the current study are available from the corresponding author on request.

Declarations

Ethics approval and consent to participate

Not applicable.

Consent for publication

All authors affirm consent for publication.

Competing interests

The authors declare that they have no competing interests.

References

[1] Penning de Vries FWT. The cost of maintenance processes in plant cells. Ann Bot. 1975;39:77–92. https://doi.org/10.1093/oxfordjournals.aob.a084919.

[2] Nelson CJ, Alexova R, Jacoby RP, Millar AH. Proteins with high turnover rate in barley leaves estimated by proteome analysis combined with in planta isotope labeling. Plant Physiol. 2014;166:91–108. https://doi.org/10.1104/pp.114.243014.

[3] Li L, Nelson CJ, Trösch J, Castleden I, Huang S, Millar AH. Protein degradation rate in *Arabidopsis thaliana* leaf growth and development. Plant Cell. 2017;29:207–28. https://doi.org/10.1105/tpc.16.00768.

[4] Chatterjee A, Abeydeera ND, Bale S, Pai P-J, Dorrestein PC, Russel DH, Ealick SE, Begley TP. *Saccharomyces cerevisiae* THI4p is a suicide thiamine thiazole synthase. Nature. 2011;478:542–6. https://doi.org/10.1038/nature10503.

[5] Fitzpatrick TB, Chapman LM. The importance of thiamine (vitamin B_1) in plant health: From crop yield to biofortification. J Biol Chem. 2020;295(34):12002–13. https://doi.org/10.1074/jbc.REV120.010918.

[6] Murata N, Takahashi S, Nishiyama Y, Allakhverdiev SI. Photoinhibition of photosystem II under environmental stress. Biochim Biophys Acta. 2007;1767:414–21. https://doi.org/10.1016/j.bbabio.2006.11.019.

[7] Tikkanen M, Mekala NR, Aro E-M. Photosystem II photoinhibition-repair cycle protects Photosystem I from irreversible damage. Biochim Biophys Acta. 2014;1837:210–5. https://doi.org/10.1016/j.bbabio.2013.10.001.

[8] Li L, Aro E-M, Millar AH. Mechanisms of photodamage and protein turnover in photoinhibition. Trends Plant Sci. 2018;23(8):667–76. https://doi.org/10.1016/j.tplants.2018.05.004.

[9] Raven JA. The cost of photoinhibition. Physiol Plant. 2011;142:87–104. https://doi.org/10.1111/j.1399-3054.2011.01465.x.

[10] Miyata K, Noguchi K, Terashima I. Cost and benefit of the repair of photodamaged photosystem II in spinach leaves: roles of acclimation to growth light. Photosynth Res. 2012;113:165–80. https://doi.org/10.1007/s11120-012-9767-0.

[11] Umena Y, Kawakami K, Shen J-R, Kamiya N. Crystal structure of oxygen-evolving photosystem II at a resolution of 1.9 Å. Nature. 2011;473:55–60. https://doi.org/10.1038/nature09913.

[12] Beisel KG, Jahnke S, Hofmann D, Köppchen S, Schurr U, Matsubara S. Continuous turnover of carotenes and chlorophyll a in mature leaves of Arabidopsis revealed by $^{14}CO_2$ pulse-chase labeling. Plant Physiol. 2010;152:2188–99. https://doi.org/10.1104/pp.109.151647.

[13] Beisel KG, Schurr U, Matsubara S. Altered turnover of β-carotene and Chl a in Arabidopsis leaves treated with lincomycin or norflurazon. Plant Cell Physiol. 2011;52(7):1193–203. https://doi.org/10.1093/pcp/pcr069.

765 [14] Thiele B, Matsubara S. Carotenoid isotopolog profiling in ^{13}C-labeled leaf extracts by LC-MS
766 and LC-FTICR-MS. In: Rodríguez-Concepción M, Welsch R, editors. *Plant and Food*
767 *Carotenoids: Methods and Protocols*, Methods in Molecular Biology. vol. 2083. New York:
768 Humana Press; 2020. p. 263–77. https://doi.org/10.1007/978-1-4939-9952-1_20.
769 [15] Jansen M, Gilmer F, Biskum B, Nagel KA, Rascher U, Fischbach A, et al. Simultaneous
770 phenotyping of leaf growth and chlorophyll fluorescence via GROWSCREEN FLUORO
771 allows detection of stress tolerance in *Arabidopsis thaliana* and other rosette plants. Funct
772 Plant BIol. 2009;36(11):902–14. https://doi.org/10.1071/FP09095.
773 [16] https://imagej.nih.gov/ij. Accessed 23 January 2019.
774 [17] Loreto F, Velikova V, Di Marco G. Respiration in the light measured by $^{12}CO_2$ emission in
775 $^{13}CO_2$ atmosphere in maize leaves. Aust J Plant Physiol. 2001;28:1003–8.
776 https://doi.org/10.1071/PP01091.
777 [18] van Breemen RB, Huang C-R, Tan Y, Sander LC, Schilling AB. Liquid chromatography/mass
778 spectrometry of carotenoids using atmospheric pressure chemical ionization. J Mass Spec.
779 1996;31:975-81.
780 https://doi.org/10.1002/(SICI)1096-9888(199609)31:9<975::AID-JMS380>3.0.CO;2-S.
781 [19] Řezanka T, Olšovská J, Sobotka M, Sigler K. The use of APCI-MS with HPLC and other
782 separation techniques for identification of carotenoids and related compounds. Curr Anal
783 Chem. 2009;5:1-25. https://doi.org/10.2174/157341109787047862.
784 [20] Kikuchi J, Shinozaki K, Hirayama T. Stable isotope labeling of *Arabidopsis thaliana* for an
785 NMR-based metabolomic approach. Plant Cell Physiol. 2004;45(8):1099–104.
786 https://doi.org/10.1093/pcp/pch117.
787 [21] Freund DM, Hegeman AD. Recent advances in stable isotope-enabled mass spectrometry-
788 based plant metabolomics. Curr Opin Biotechnol. 2017;43:41–8.
789 https://doi.org/10.1016/j.copbio.2016.08.002.
790 [22] Jang C, Chen L, Rabinowitz JD. Metabolomics and isotope tracing. Cell. 2018; 173:822–37.
791 https://doi.org/10.1016/j.cell.2018.03.055.
792 [23] Allen DK, Libourel IG, Shachar-Hill Y. Metabolic flux analysis in plants: coping with
793 complexity. Plant Cell Environ. 2009;32:1241–57.
794 https://doi.org/10.1111/j.1365-3040.2009.01992.x.
795 [24] Shih M-L, Morgan JA. Metabolic flux analysis of secondary metabolism in plants. Metab Eng
796 Commun. 2020;10:e00123. https://doi.org/10.1016/j.mec.2020.e00123.
797 [25] Wieloch T. The next phase in the development of ^{13}C isotopically non-stationary metabolic
798 flux analysis. J Exp Bot. 2021;72(18):6087-90. https://doi.org/10.1093/jxb/erab292.
799 [26] Kruger NJ, Ratchliffe RG. Whither metabolic flux analysis in plants? J Exp Bot. 2021.
800 https://doi.org/10.1093/jxb/erab389.
801 [27] Hasunuma T, Harada K, Miyazawa S-I, Kondo A, Fukusaki E, Miyake C. Metabolic turnover
802 analysis by a combination of in vivo ^{13}C-labelling from $^{13}CO_2$ and metabolic profiling with

CE-MS/MS reveals rate-limiting steps of the C_3 photosynthetic pathway in *Nicotiana tabacum* leaves. J Exp Bot. 2010;61(4):1041–51. https://doi.org/10.1093/jxb/erp374.

[28] Szecowka M, Heise R, Tohge T, Nunes-Nesi A, Vosloh D, Huege J, Feil R, Lunn J, Nikoloski Z, Stitt M, Fernie AR, Arrivault S. Metabolic fluxes in an illuminated *Arabidopsis* rosette. Plant Cell. 2013;25:694–714. https://doi.org/10.1105/tpc.112.106989.

[29] Ma F, Jazmin LJ, Young JD, Allen DK. Isotopically nonstationary ^{13}C flux analysis of changes in *Arabidopsis thaliana* leaf metabolism due to high light acclimation. Proc Natl Acad Sci USA. 2014;111(47):16967–72. https://doi.org/10.1073/pnas.1319485111.

[30] Arrivault S, Obata T, Szecówka M, Mengin V, Guenther M, Hoehne M, Fernie AR, Stitt M. Metabolite pools and carbon flow during C_4 photosynthesis in maize: $^{13}CO_2$ labeling kinetics and cell type fractionation. J Exp Bot. 2017;68(2):283–98. https://doi.org/10.1093/jxb/erw414.

[31] Abadie C, Tcherkez G. ^{13}C isotope labelling to follow the flux of photorespiratory intermediates. Plants. 2021;10:427. https://doi.org/10.3390/plants10030427.

[32] González-Cabanelas D, Wright LP, Paetz C, Onkokesung N, Gershenzon J, Rodríguez-Concepción M, Phillips MA. The diversion of 2-*C*-methyl-D-erythritol-2,4-cyclodiphosphate from the 2-*C*-methyl-D-erythritol 4-phosphate pathway to hemiterpene glycosides mediates stress responses in *Arabidopsis thaliana*. Plant J. 2015;82:122–37. https://doi.org/10.1111/tpj.12798.

[33] Bergman ME, González-Cabanelas D, Wright LP, Walker BJ, Phillips MA. Isotope ratio-based quantification of carbon assimilation highlights the role of plastidial isoprenoid precursor availability in photosynthesis. Plant Methods. 2021;17:32. https://doi.org/10.1186/s13007-021-00731-8.

[34] Delwiche CF, Sharkey TD. Rapid appearance of ^{13}C in biogenic isoprene when $^{13}CO_2$ is fed to intact leaves. Plant Cell Physiol. 1993;16:587–91. https://doi.org/10.1111/j.1365-3040.1993.tb00907.x.

[35] Karl T, Fall R, Rosenstiel TN, Prazeller P, Larsen B, Seufert G, Lindinger W. On-line analysis of the $^{13}CO_2$ labeling of leaf isoprene suggests multiple subcellular origins of isoprene precursors. Planta. 2002;215:894–905. https://doi.org/10.1007/s00425-002-0825-2.

[36] Ghirardo A, Wright LP, Bi Z, Rosenkranz M, Pulido P, Rodríguez-Concepción M, Niinemets Ü, Brüggemann N, Gershenzon J, Schnitzler J-P. Metabolic flux analysis of plastidic isoprenoid biosynthesis in poplar leaves emitting and nonemitting isoprene. Plant Physiol. 2014;165:37–51. https://doi.org/10.1104/pp.114.236018.

[37] Kagawa A, Sugimoto A, Maximov TC. Seasonal course of translocation, storage and remobilization of ^{13}C pulse-labeled photoassimilate in naturally growing *Larix gmelinii* saplings. New Phytol. 2006;171:793–804. https://doi.org/10.1111/j.1469-8137.2006.01780.x.

[38] Högberg P, Högberg MN, Göttlicher SG, Betson NR, Keel SG, Metcalfe DB, Campbell C, Schindlbacher A, Hurry V, Lundmark T, Linder S, Näsholm T. High temporal resolution tracing of photosynthate carbon from the tree canopy to forest soil microorganisms. New Phytol. 2008;177:220–8. https://doi.org/10.1111/j.1469-8137.2007.02238.x.

[39] Epron D, Ngao J, Dannoura M, Bakker RM, Zeller B, Bazot S, Bosc A, Plain C, Lara J-C, Priault P, Barthes L, Loustau D. Seasonal variations of belowground carbon transfer assessed by in situ $^{13}CO_2$ pulse labelling of trees. Biogeosciences. 2011;8:1153–68. https://doi.org/10.5194/bg-8-1153-2011.

[40] Kuptz D, Fleischmann F, Matyssek R, Grams TEE. Seasonal patterns of carbon allocation to respiratory pools in 60-yr-old deciduous (*Fagus sylvatica*) and evergreen (*Picea abies*) trees assessed via whole-tree stable carbon isotope labeling. New Phytol. 2011;191:160–72. https://doi.org/10.1111/j.1469-8137.2011.03676.x.

[41] Dersch LM, Beckers V, Rasch D, Melzer G, Bolten C, Kiep K, Becker H, Bläsing OE, Fuchs R, Ehrhardt T, Wittmann C. Novel approach for high-throughput metabolic screening of whole plants by stable isotopes. Plant Physiol. 2016;171:25–41. https://doi.org/10.1104/pp.15.01217.

[42] Chen W-P, Yang X-Y, Harms GL, Gray WM, Hegeman AD, Cohen JD. An automated growth enclosure for metabolic labeling of *Arabidopsis thaliana* with ^{13}C-carbon dioxide – an *in vivo* labeling system for proteomics and metabolomics research. Proteome Sci. 2011;9:9. https://doi.org/10.1186/1477-5956-9-9.

[43] Ishihara H, Moraes TA, Arrivault S, Stitt M. Assessing protein synthesis and degradation rates in *Arabidopsis thaliana* using amino acid analysis. Curr Protoc. 2021;1:e114. https://doi.org/10.1002/cpz1.114.

[44] Huege J, Sulpice R, Gibon Y, Lisec J, Koehl K, Kopka J. GC-EI-TOF-MS analysis of in vivo carbon-partitioning into soluble metabolite pools of higher plants by monitoring isotope dilution after $^{13}CO_2$ labelling. Phytochemistry. 2007;68:2257–72. https://doi.org/10.1016/j.phytochem.2007.03.026.

[45] Gleichenhagen M, Zimmermann BF, Herzig B, Janzik I, Jahnke S, Boner M, Stehle P, Galensa R. Intrinsic isotopic ^{13}C labelling of polyphenols. Food Chem. 2013;141(3):2582–90. https://doi.org/10.1016/j.foodchem.2013.05.070.

[46] Amunts A, Toporik H, Borovikova A, Nelson N. Structure determination and improved model of plant photosystem I. J Biol Chem. 2010;285(5):3478–86. https://doi.org/10.1074/jbc.M109.072645.

[47] Demmig-Adams B. Survey of thermal energy dissipation and pigment composition in sun and shade leaves. Plant Cell Physiol. 1998;39(5):474–82. https://doi.org/10.1093/oxfordjournals.pcp.a029394.

[48] Matsubara S, Krause GH, Aranda J, Virgo A, Beisel KG, Jahns P, Winter K. Sun-shade patterns of leaf carotenoid composition in 86 species of neotropical forest plants. Funct Plant Biol. 2009;36:20–36. https://doi.org/10.1071/FP08214.

880 [49] Ashikawa I, Miyata A, Koike H, Inoue Y, Koyama Y. Light-induced structural change of β-
881 carotene in thylakoid membranes. Biochemistry. 1986;25:6154–60.
882 https://doi.org/10.1021/bi00368a049.
883 [50] Milanowska J, Gruszecki WI. Heat-induced and light-induced isomerization of the xanthophyll
884 pigment zeaxanthin. J Photochem Photobiol B. 2005;80(3):178–86.
885 https://doi.org/10.1016/j.jphotobiol.2005.05.004.
886 [51] Sander LC, Epler Sharpless K, Craft NE, Wise SA. Development of engineered stationary
887 phases for the separation of carotenoid isomers. Anal Chem. 1994;66:1667–74.
888 https://doi.org/10.1021/ac00082a012.
889 [52] Emenhiser C, Simunovic N, Sander LC, Schwartz SJ. Separation of geometrical carotenoid
890 isomers in biological extracts using a polymeric C_{30} column in reversed-phase liquid
891 chromatography. J Agric Food Chem. 1996;44:3887–93.
892 https://doi.org/10.1016/0021-9673(95)00336-L.
893 [53] Zhang H, Huang D, Cramer WA. Stoichiometrically bound *β*-carotene in the cytochrome *b_6f*
894 complex of oxygenic photosynthesis protects against oxygen damage. J Biol Chem.
895 1999;274(3):1581–7. https://doi.org/10.1074/jbc.274.3.1581.
896 [54] Kurisu G, Zhang H, Smith JL, Cramer WA. Structure of the cytochrome b_6f complex of
897 oxygenic photosynthesis: Tuning the cavity. Science 2003;302:1009–14.
898 https://doi.org/10.1126/science.1090165.
899 [55] Malone LA, Qian P, Mayneord GE, Hitchcock A, Farmer DA, Thompson RF, Swainsbury
900 DJK, Ranson NA, Hunter CN, Johnson MP. Cryo-EM structure of the spinach cytochrome
901 *b_6f* complex at 3.6 Å resolution. Nature. 2019;575:535–9.
902 https://doi.org/10.1038/s41586-019-1746-6.
903 [56] Liu Z, Yan H, Wang K, Kuang T, Zhang J, Gui L, An X, Chang W. Crystal structure of spinach
904 major light-harvesting complex at 2.72 Å resolution. Nature. 2004;428:287–92.
905 https://doi.org/10.1038/nature02373.
906 [57] Caffarri S, Passarini F, Bassi R, Croce R. A specific binding site for neoxanthin in the
907 monomeric antenna proteins CP26 and CP29 of photosystem II. FEBS Lett.
908 2007;581:4704–10. https://doi.org/10.1016/j.febslet.2007.08.066.
909 [58] Pan X, Li M, Wan T Wang L, Jia C, Hou Z, Zhao X, Zhang J, Chang W. Structural insights
910 into energy regulation of light-harvesting complex CP29 from spinach. Nat Struct Mol Biol.
911 2011;18(3):309–15. https://doi.org/10.1038/nsmb.2008.
912 [59] Wei X, Su X, Cao P, Liu X, Chang W, Li M, Zhang X, Liu Z. Structure of spinach photosystem
913 II-LHCII supercomplex at 3.2 Å resolution. Nature. 2016;534:69–74.
914 https://doi.org/10.1038/nature18020.
915 [60] Vavilin D, Vermaas W. Continuous chlorophyll degradation accompanied by chlorophyllide
916 and phytol reutilization for chlorophyll synthesis in *Synechocystis* sp. PCC 6803. Biochim
917 Biophys Acta. 2007;1767:920–9. https://doi.org/10.1016/j.bbabio.2007.03.010.

[61] Ischebeck T, Zbierzak AM, Kanwischer M, Dörmann P. A salvage pathway for phytol metabolism in *Arabidopsis*. J Biol Chem. 2006;281(5):24707. https://doi.org/10.1074/jbc.M509222200.

[62] Holčapek M, Jirásko R, Lísa M. Basic rules for the interpretation of atmospheric pressure ionization mass spectra of small molecules. J Chromatogr A. 2010;1217:3908–21. https://doi.org/10.1016/j.chroma.2010.02.049.

[63] Croce R, van Amerongen H. Light-harvesting in photosystem I. Photosynth Res. 2013;116:153–66. https://doi.org/10.1007/s11120-013-9838-x.

Figure legends

Fig. 1. Schematic overview of the $^{13}CO_2$ labeling chamber. The devices to control CO_2 concentration (mass flow controller, MFC) and air humidity (dew point trap) are depicted along with the sensors for CO_2 (infrared gas analyzer, IRGA), temperature, humidity, light intensity and pressure. The colored background shows the chamber area (top view). The arrows indicate the directions of air (or water) flow. The size of the arrows and the thickness of the lines correspond to the inner diameter of tubing (polytetrafluoroethylene or metal).

Fig. 2. Plant positions in the labeling chamber. **a** The positions of 15 plants (P1–P15) and the light intensity (in µmol photon m^{-2} s^{-1}) distribution measured in and around each plant position without the glass cover of the labeling chamber. The light intensity thus measured was ranging between 204 (P15) and 279 (P7) µmol photon m^{-2} s^{-1} among the 15 positions, with the mean intensity of 238 µmol photon m^{-2} s^{-1}. **b** A picture of the closed labeling chamber with 15 Arabidopsis plants placed under LED lamps in a controlled climate chamber. The bottom of the plant cups (see Additional file 1; Fig. A1 for description of the plant cup) was touching the water in a shallow basin attached to the lower surface of the chamber body. The basin can be filled and drained through watering tubes (seen in the front) without opening the chamber.

Fig. 3. Concentrations of photosynthetic pigments in Arabidopsis plants harvested in the early morning of day 8. **a** Lutein (Lut) and all-*trans*-β-carotene (β-Car). **b** Zeaxanthin (Zea) and antheraxanthin (Anthera). **c** Violaxanthin (Vio) and neoxanthin (Neo). Carotenoid levels relative to the total chlorophyll content (mmol mol^{-1} Chl) are shown. **d** De-epoxidation state (DES) of the xanthophyll cycle calculated as (Anthera + Zea)/(Vio + Anthera + Zea). **e** Chlorophyll *a* (Chl *a*) and chlorophyll *b* (Chl *b*) contents per unit leaf mass (µmol g^{-1} fresh weight). Black triangles represent control plants (n=4) that stayed in the ambient air outside the

labeling chamber. For ^{13}C-labeled samples, red and blue symbols are for plants with higher (n=12) or lower (n=3) ^{13}C incorporation in the pigments, respectively. The latter showed visible stress symptoms (see Additional file 1; Fig. A3b for images of the plants). The box plots are based on all data. The thick horizontal line inside the box shows the median. The middle 50% of the data fall between the upper and lower end of the box. Data beyond the whisker boundaries are outliers.

Fig. 4. Chromatograms of a ^{13}C-labeled Arabidopsis leaf pigment sample obtained by LC-TQ-MS. **a** Pigment separation monitored at 440 nm. The pigment peaks are numbered as follows: 1, Vio; 2, 9-*cis*-Neo; 3, Anthera; 4, Chl *b*; 5, Lut; 6, Zea (if present); 7, Chl *a*; 8, all-*trans*-β-Car; 9, 9-*cis*-β-Car. This sample had a very small amount of Anthera and hardly any Zea. In the same sample, selected ions were monitored at specific mass-to-charge (m/z) values: **b** Vio and 9-*cis*-Neo; **c** Anthera; **d** Chl *b*; **e** Lut (and Zea if present); **f** Chl *a*; **g** all-*trans*- and 9-*cis*-β-Car. Xanthophylls, especially Lut, tend to lose water upon protonation in positive ion mode.

Fig. 5. Mass spectra of all-*trans*-β-Car extracted from non-labeled and ^{13}C-labeled Arabidopsis plants. FTICR-MS showing two types of quasi-molecular ions of β-Car, $[M]^+$ and $[M+H]^+$, in a non-labeled (**a**) and a ^{13}C-labeled (**c**) sample. Deviations from the expected mass (Δ) are given in parts per million (ppm). TQ-MS in the same non-labeled (**b**) and ^{13}C-labeled (**d**) samples as in **a** and **c**. Overlapping mass peaks of $[M]^+$ and $[M+H]^+$ ions are regarded as $[M+H]^+$ or $[M]^+$ in the analysis of FTICR-MS and TQ-MS, respectively. Peak assignment of these data is summarized in Additional file 2; Tables A3–A6. Theoretical distribution of carotenoid isotopologs based on natural ^{13}C abundance (~1.1%) is presented in Additional file 1; Fig. A8.

Fig. 6. Mass spectra of Lut extracted from non-labeled and ^{13}C-labeled Arabidopsis plants. FTICR-MS showing four different types of quasi-molecular ions of Lut, $[M+H-2H_2O]^+$, $[M+H-H_2O]^+$, $[M]^+$ and $[M+H]^+$, in a non-labeled (**a**) and a ^{13}C-labeled (**c**) sample. Small peaks of ^{13}C-labeled $[M+H-2H_2O]^+$ ion were detected in the same m/z region as non-labelled $[M]^+$ and $[M+H]^+$ ions in **c**. Deviations from the expected mass (Δ) are given in ppm. TQ-MS showing four types of quasi-molecular ions, $[M+H-2H_2O]^+$, $[M+H-H_2O]^+$, $[M]^+$ and $[M+H]^+$, in the same non-labeled (**b**) and ^{13}C-labeled (**d**) samples as in **a** and **c**. Since TQ-MS cannot separate overlapping peaks of non-labeled $[M]^+$ and $[M+H]^+$ at m/z 569–571 and ^{13}C-labeled $[M]^+$ and $[M+H]^+$ at m/z 607–608, they are regarded as $[M+H]^+$. Peak assignment of these data is summarized in Additional file 2; Tables A7–A10.

Fig. 7. Mass spectra of Chl *a* extracted from non-labeled and ^{13}C-labeled Arabidopsis plants. FTICR-MS showing three types of quasi-molecular ions of Chl *a*, $[M]^+$, $[M+H]^+$ and $[M+K]^+$, in a non-labeled (**a**) and a ^{13}C-labeled (**c**) sample. Deviations from the expected mass (Δ) are given in ppm. TQ-MS showing two types of quasi-molecular ions, $[M+H]^+$ and $[M+K]^+$, in the same non-labeled (**b**) and ^{13}C-labeled (**d**) samples as in **a** and **c**. The $[M]^+$ peak was hardly detected and thus not considered in the analysis of TQ-MS data. Mass peaks of ^{13}C-labeled $[M+H]^+$ and non-labeled $[M+K]^+$ were overlapping at *m/z* 931–933 in **d**. The contribution of non-labeled $[M+K]^+$ in this *m/z* region was estimated from the intensity of non-labeled $[M+H]^+$ peaks and the ratio between $[M+H]^+$ and $[M+K]^+$ peaks found in **b** (1:0.26). For Chl, natural abundance of Mg isotopes (^{24}Mg 79%, ^{25}Mg 10% and ^{26}Mg 11%) was taken into account to calculate their contributions to each mass peak. The estimated peak intensity of ^{24}Mg-Chl as $[M+H]^+$ was then considered representative of Chl *a* in the analysis of TQ-MS data. Peak assignment of these data is summarized in Additional file 2; Tables A11–A14.

Fig. 8. Mass spectra of Chl *b* extracted from non-labeled and ^{13}C-labeled Arabidopsis leaves. FTICR-MS showing two types of quasi-molecular ions of Chl *b*, $[M]^+$ and $[M+H]^+$, in a non-labeled (**a**) and a ^{13}C-labeled (**c**) sample. Deviations from the expected mass (Δ) are given in ppm. TQ-MS showing two types of quasi-molecular ions, $[M+H]^+$ and $[M+K]^+$, in the same non-labeled (**b**) and ^{13}C-labeled (**d**) samples as in **a** and **c**. The $[M]^+$ peak was hardly detected and thus not considered in the analysis of TQ-MS data. Mass peaks of ^{13}C-labeled $[M+H]^+$ and non-labeled $[M+K]^+$ were overlapping at *m/z* 945–948 in **d**. The contribution of non-labeled $[M+K]^+$ in this *m/z* region was estimated from the intensity of non-labeled $[M+H]^+$ peaks and the ratio between $[M+H]^+$ and $[M+K]^+$ peaks found in **b** (1:0.74). For Chl, natural abundance of Mg isotopes (^{24}Mg 79%, ^{25}Mg 10% and ^{26}Mg 11%) was taken into account to calculate their contributions to each mass peak. The estimated mass peak intensity of ^{24}Mg-Chl as $[M+H]^+$ was then considered representative of Chl *b* in the analysis of TQ-MS data. Peak assignment of these data is summarized in Additional file 2; Tables A15-A18.

Fig. 9. Labeled and non-labeled pigments in ^{13}C-labeled Arabidopsis leaves harvested after 7-d $^{13}CO_2$ labeling. **a** Degree of ^{13}C labeling (ΣDoL) and **b** non-labeled pigment population (NLP) of all-*trans*- and 9-*cis*-β-Car, Lut, Chl *a* and Chl *b*. Red and blue symbols represent plants that had higher (n=12) or lower (n=3) ^{13}C incorporation in pigments, respectively. Black triangles in **a** are control plants (n=4) that stayed in the ambient air outside the labeling chamber. Data of the control plants are not shown in **b** since they all had 100% NLP. The box plots are based on the data of the ^{13}C-labeled samples (i.e., red and blue symbols); the control plants (black

triangles) shown in **a** are not included in the box plots. The thick horizontal line inside the box shows the median. The middle 50% of the data fall between the upper and lower end of the box. Data beyond the whisker boundaries are outliers.

Fig. 10. Correlation between non-labeled population (NLP) of pigments extracted from Arabidopsis leaves after 7-d $^{13}CO_2$ labeling. **a** Chl *a* and Chl *b*. **b** All-*trans*-β-Car and Lut. **c** Chl *a* and all-*trans*-β-Car. **d** Chl *b* and Lut. Red and blue symbols represent plants that had higher (n=12) or lower (n=3) ^{13}C incorporation in pigments, respectively.

Figures

Figure 1

Schematic overview of the $^{13}CO_2$ labeling chamber. The devices to control CO_2 concentration (mass flow controller, MFC) and air humidity (dew point trap) are depicted along with the sensors for CO_2 (infrared gas analyzer, IRGA), temperature, humidity, light intensity and pressure. The colored background shows the chamber area (top view). The arrows indicate the directions of air (or water) flow. The size of the arrows and the thickness of the lines correspond to the inner diameter of tubing (polytetrafluoroethylene or metal).

Figure 2

Plant positions in the labeling chamber. **a** The positions of 15 plants (P1–P15) and the light intensity (in µmol photon m^{-2} s^{-1}) distribution measured in and around each plant position without the glass cover of the labeling chamber. The light intensity thus measured was ranging between 204 (P15) and 279 (P7) µmol photon m^{-2} s^{-1} among the 15 positions, with the mean intensity of 238 µmol photon m^{-2} s^{-1}. **b** A picture of the closed labeling chamber with 15 Arabidopsis plants placed under LED lamps in a controlled climate chamber. The bottom of the plant cups (see Additional file 1; Fig. A1 for description of the plant cup) was touching the water in a shallow basin attached to the lower surface of the chamber body. The basin can be filled and drained through watering tubes (seen in the front) without opening the chamber.

Figure 3

Concentrations of photosynthetic pigments in Arabidopsis plants harvested in the early morning of day 8. **a** Lutein (Lut) and all-*trans*-β-carotene (β-Car). **b** Zeaxanthin (Zea) and antheraxanthin (Anthera). **c** Violaxanthin (Vio) and neoxanthin (Neo). Carotenoid levels relative to the total chlorophyll content (mmol mol^{-1} Chl) are shown. **d** De-epoxidation state (DES) of the xanthophyll cycle calculated as (Anthera + Zea)/(Vio + Anthera + Zea). **e** Chlorophyll *a* (Chl *a*) and chlorophyll *b* (Chl *b*) contents per unit leaf mass (µmol g^{-1} fresh weight). Black triangles represent control plants (n=4) that stayed in the ambient air outside the labeling chamber. For ^{13}C-labeled samples, red and blue symbols are for plants with higher (n=12) or lower (n=3) ^{13}C incorporation in the pigments, respectively. The latter showed visible stress

symptoms (see Additional file 1; Fig. A3b for images of the plants). The box plots are based on all data. The thick horizontal line inside the box shows the median. The middle 50% of the data fall between the upper and lower end of the box. Data beyond the whisker boundaries are outliers.

Figure 4

Chromatograms of a ^{13}C-labeled Arabidopsis leaf pigment sample obtained by LC-TQ-MS. **a** Pigment separation monitored at 440 nm. The pigment peaks are numbered as follows: 1, Vio; 2, 9-*cis*-Neo; 3, Anthera; 4, Chl *b*; 5, Lut; 6, Zea (if present); 7, Chl *a*; 8, all-*trans*-β-Car; 9, 9-*cis*-β-Car. This sample had a very small amount of Anthera and hardly any Zea. In the same sample, selected ions were monitored at specific mass-to-charge (*m*/*z*) values: **b** Vio and 9-*cis*-Neo; **c** Anthera; **d** Chl *b*; **e** Lut (and Zea if present); **f** Chl *a*; **g** all-*trans*- and 9-*cis*-β-Car. Xanthophylls, especially Lut, tend to lose water upon protonation in positive ion mode.

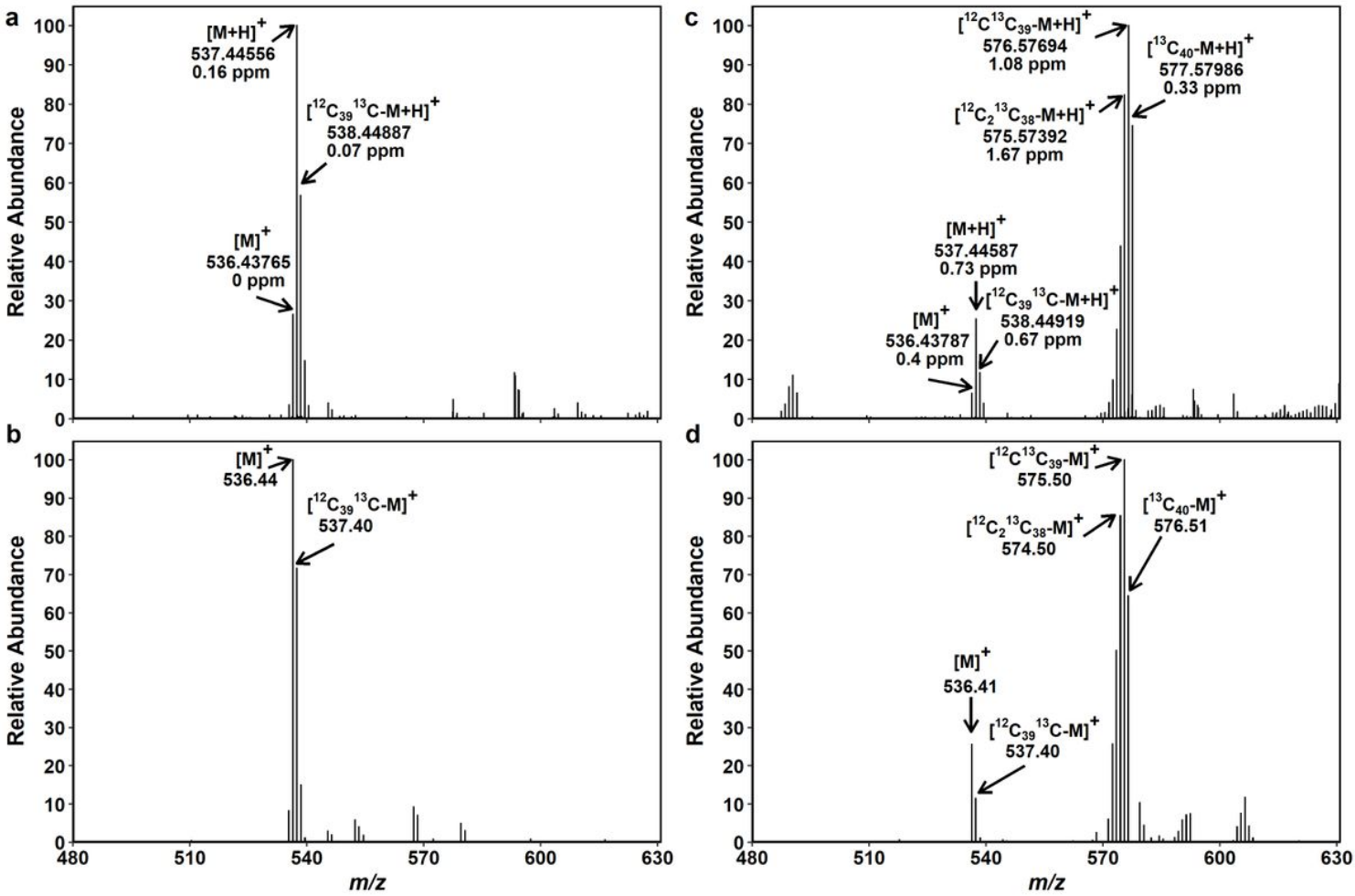

Figure 5

Mass spectra of all-*trans*-β-Car extracted from non-labeled and ^{13}C-labeled Arabidopsis plants. FTICR-MS showing two types of quasi-molecular ions of β-Car, $[M]^+$ and $[M+H]^+$, in a non-labeled (**a**) and a ^{13}C-labeled (**c**) sample. Deviations from the expected mass (Δ) are given in parts per million (ppm). TQ-MS in the same non-labeled (**b**) and ^{13}C-labeled (**d**) samples as in **a** and **c**. Overlapping mass peaks of $[M]^+$ and $[M+H]^+$ ions are regarded as $[M+H]^+$ or $[M]^+$ in the analysis of FTICR-MS and TQ-MS, respectively. Peak assignment of these data is summarized in Additional file 2; Tables A3–A6. Theoretical distribution of carotenoid isotopologs based on natural ^{13}C abundance (~1.1%) is presented in Additional file 1; Fig. A8.

Figure 6

Mass spectra of Lut extracted from non-labeled and ^{13}C-labeled Arabidopsis plants. FTICR-MS showing four different types of quasi-molecular ions of Lut, $[M+H-2H_2O]^+$, $[M+H-H_2O]^+$, $[M]^+$ and $[M+H]^+$, in a non-labeled (**a**) and a ^{13}C-labeled (**c**) sample. Small peaks of ^{13}C-labeled $[M+H-2H_2O]^+$ ion were detected in the same *m/z* region as non-labelled $[M]^+$ and $[M+H]^+$ ions in **c**. Deviations from the expected mass (Δ) are given in ppm. TQ-MS showing four types of quasi-molecular ions, $[M+H-2H_2O]^+$, $[M+H-H_2O]^+$, $[M]^+$ and $[M+H]^+$, in the same non-labeled (**b**) and ^{13}C-labeled (**d**) samples as in **a** and **c**. Since TQ-MS cannot separate overlapping peaks of non-labeled $[M]^+$ and $[M+H]^+$ at *m/z* 569–571 and ^{13}C-labeled $[M]^+$ and $[M+H]^+$ at *m/z* 607–608, they are regarded as $[M+H]^+$. Peak assignment of these data is summarized in Additional file 2; Tables A7–A10.

Figure 7

Mass spectra of Chl *a* extracted from non-labeled and ^{13}C-labeled Arabidopsis plants. FTICR-MS showing three types of quasi-molecular ions of Chl *a*, $[M]^+$, $[M+H]^+$ and $[M+K]^+$, in a non-labeled (**a**) and a ^{13}C-labeled (**c**) sample. Deviations from the expected mass (Δ) are given in ppm. TQ-MS showing two types of quasi-molecular ions, $[M+H]^+$ and $[M+K]^+$, in the same non-labeled (**b**) and ^{13}C-labeled (**d**) samples as in **a** and **c**. The $[M]^+$ peak was hardly detected and thus not considered in the analysis of TQ-MS data. Mass peaks of ^{13}C-labeled $[M+H]^+$ and non-labeled $[M+K]^+$ were overlapping at *m/z* 931–933 in **d**. The contribution of non-labeled $[M+K]^+$ in this *m/z* region was estimated from the intensity of non-labeled $[M+H]^+$ peaks and the ratio between $[M+H]^+$ and $[M+K]^+$ peaks found in **b** (1:0.26). For Chl, natural abundance of Mg isotopes (^{24}Mg 79%, ^{25}Mg 10% and ^{26}Mg 11%) was taken into account to calculate their contributions to each mass peak. The estimated peak intensity of ^{24}Mg-Chl as $[M+H]^+$ was then

considered representative of Chl *a* in the analysis of TQ-MS data. Peak assignment of these data is summarized in Additional file 2; Tables A11–A14.

Figure 8

Mass spectra of Chl *b* extracted from non-labeled and ^{13}C-labeled Arabidopsis leaves. FTICR-MS showing two types of quasi-molecular ions of Chl *b*, $[M]^+$ and $[M+H]^+$, in a non-labeled (**a**) and a ^{13}C-labeled (**c**) sample. Deviations from the expected mass (Δ) are given in ppm. TQ-MS showing two types of quasi-molecular ions, $[M+H]^+$ and $[M+K]^+$, in the same non-labeled (**b**) and ^{13}C-labeled (**d**) samples as in **a** and **c**. The $[M]^+$ peak was hardly detected and thus not considered in the analysis of TQ-MS data. Mass peaks of ^{13}C-labeled $[M+H]^+$ and non-labeled $[M+K]^+$ were overlapping at *m/z* 945–948 in **d**. The contribution of non-labeled $[M+K]^+$ in this *m/z* region was estimated from the intensity of non-labeled $[M+H]^+$ peaks and the ratio between $[M+H]^+$ and $[M+K]^+$ peaks found in **b** (1:0.74). For Chl, natural abundance of Mg isotopes (^{24}Mg 79%, ^{25}Mg 10% and ^{26}Mg 11%) was taken into account to calculate their contributions to each mass peak. The estimated mass peak intensity of ^{24}Mg-Chl as $[M+H]^+$ was then considered representative of Chl *b* in the analysis of TQ-MS data. Peak assignment of these data is summarized in Additional file 2; Tables A15-A18.

Figure 9

Labeled and non-labeled pigments in ^{13}C-labeled Arabidopsis leaves harvested after 7-d $^{13}CO_2$ labeling. **a** Degree of ^{13}C labeling (ΣDoL) and **b** non-labeled pigment population (NLP) of all-*trans*- and 9-*cis*-β-Car, Lut, Chl *a* and Chl *b*. Red and blue symbols represent plants that had higher (*n*=12) or lower (*n*=3) ^{13}C incorporation in pigments, respectively. Black triangles in **a** are control plants (*n*=4) that stayed in the ambient air outside the labeling chamber. Data of the control plants are not shown in **b** since they all had 100% NLP. The box plots are based on the data of the ^{13}C-labeled samples (i.e., red and blue symbols); the control plants (black triangles) shown in **a** are not included in the box plots. The thick horizontal line inside the box shows the median. The middle 50% of the data fall between the upper and lower end of the box. Data beyond the whisker boundaries are outliers.

Figure 10

Correlation between non-labeled population (NLP) of pigments extracted from Arabidopsis leaves after 7-d $^{13}CO_2$ labeling. **a** Chl *a* and Chl *b*. **b** All-*trans*-β-Car and Lut. **c** Chl *a* and all-*trans*-β-Car. **d** Chl *b* and Lut. Red and blue symbols represent plants that had higher (*n*=12) or lower (*n*=3) ^{13}C incorporation in pigments, respectively.

Supplementary Files

This is a list of supplementary files associated with this preprint. Click to download.

- Additionalfile1.pdf
- Additionalfile2.pdf